RSC Advances

REVIEW

View Article Online
View Journal | View Issue

Cite this: *RSC Adv.*, 2025, **15**, 10395

Progress of FeP anode materials for alkali metal ion batteries

Jiakun Xia,[a] Jiaxin Guo,[a] Shengkai Li, *[a] Hui Liu,[a] Jinliang Lin,[a] Donghui Liu,[a] Yao Liu,[a] Qi Wang,[a] Bin Feng[a] and Xianming Xia[b]

FeP is a promising insertion–conversion electrode material. It has been demonstrated that this material exhibits several noteworthy physicochemical properties, including a high theoretical capacity, low cost, and good mechanical and thermal stability. Furthermore, its low insertion potential and high theoretical capacity of up to 926 mA h g^{-1} have attracted the attention of researchers as a potential electrode material for alkali metal ion batteries (AMIB). However, the material also exhibits certain disadvantages, including a considerable voltage hysteresis, a substantial volume change, and suboptimal reaction kinetics, resulting in a relatively low-rate capacity and accelerated capacity decay. However, some effective strategies such as composite, doping, and nanostructuring have shown promising applications. Here we present a timely and systematic review of the latest research and significant advances in FeP and its composites, covering synthesis, electrode design, and applications (especially in advanced lithium/sodium/potassium ion batteries) and their reaction mechanisms. Consequently, further modifications have been devised for using iron phosphide composites as anode materials for alkali metal ion batteries (AMIB). The continued innovation of FeP-based anodes demonstrates promise for their utilization in large-scale energy storage applications, including grid storage and electric vehicles. Furthermore, there is an aspiration to encourage the ongoing advancement of FeP anode materials for the development of advanced rechargeable ion batteries.

Received 22nd January 2025
Accepted 20th March 2025

DOI: 10.1039/d5ra00525f

rsc.li/rsc-advances

1 Introduction

With the rapid social and economic development of mankind, the energy demand is increasing day by day. The growing environmental threat stems from the continuous exploitation of fossil fuels as the main source of energy, and the overuse of fossil fuels, such as coal, oil, and natural gas, which has led to the emergence of problems including global warming and pollution.[1–5] In response to the depletion of fossil fuels, natural resources such as wind, solar, geothermal, and tidal energy are considered promising candidates for generating and supplying electricity. As a result, a great deal of research has been aimed at replacing fossil fuels with clean, renewable energy sources such as solar, wind, and geothermal energy.[6–11] Solar panels and wind turbines have been widely installed, but unpredictable weather and climate fluctuations remain a major obstacle to their widespread use. Whereas the development and application of electrical energy storage and conversion systems (EESCS) have greatly facilitated the storage and utilization of clean energy, alkali metal-ion batteries (AMIBs) have attracted much attention due to their considerable power density, and have been reported to be used in portable electronics, electric vehicles, and smart grids.[12–17]

Alkali metal ion batteries (AMIBs) are gaining traction as high-performance energy storage systems for applications spanning consumer electronics, electric vehicles, and energy grids. Characterized by high energy density and light weight, AMIBs represent a frontier in rechargeable battery technology. Nevertheless, the landscape of AMIB development is fraught with challenges. Electrode materials, the linchpin of AMIB performance, often fall short in terms of capacity, suffer from volume expansion during (de)lithium/sodium/potassium, and experience diminished cyclic stability. This paper will scrutinize the progression of AMIBs and the quest for advanced electrode materials (Fig. 1).

Among the AMIBs that have been reported so far, the commercialization of lithium-ion batteries (LIBs) was used by Sony in electronics as early as 1991, which has led to the continued expansion of applications in electric vehicles (EVs) and portable power sources due to the significant advantages of high energy density, good cycling characteristics, high reversible capacity, and low memory effect.[18–20] However, the scarcity and uneven geographical distribution of lithium resources are important challenges in the current global energy transition. Alternatives to Li-ion batteries, including sodium-ion batteries

[a]School of Intelligent Manufacturing and Materials Engineering, Gannan University of Science and Technology, Ganzhou, 341000, China. E-mail: shengkai_li@yeah.net
[b]Hunan Provincial Key Laboratory of Xiangnan Rare-Precious Metals Compounds and Applications, College of Chemistry and Environmental Science, Xiangnan University, Chenzhou, 423000, China

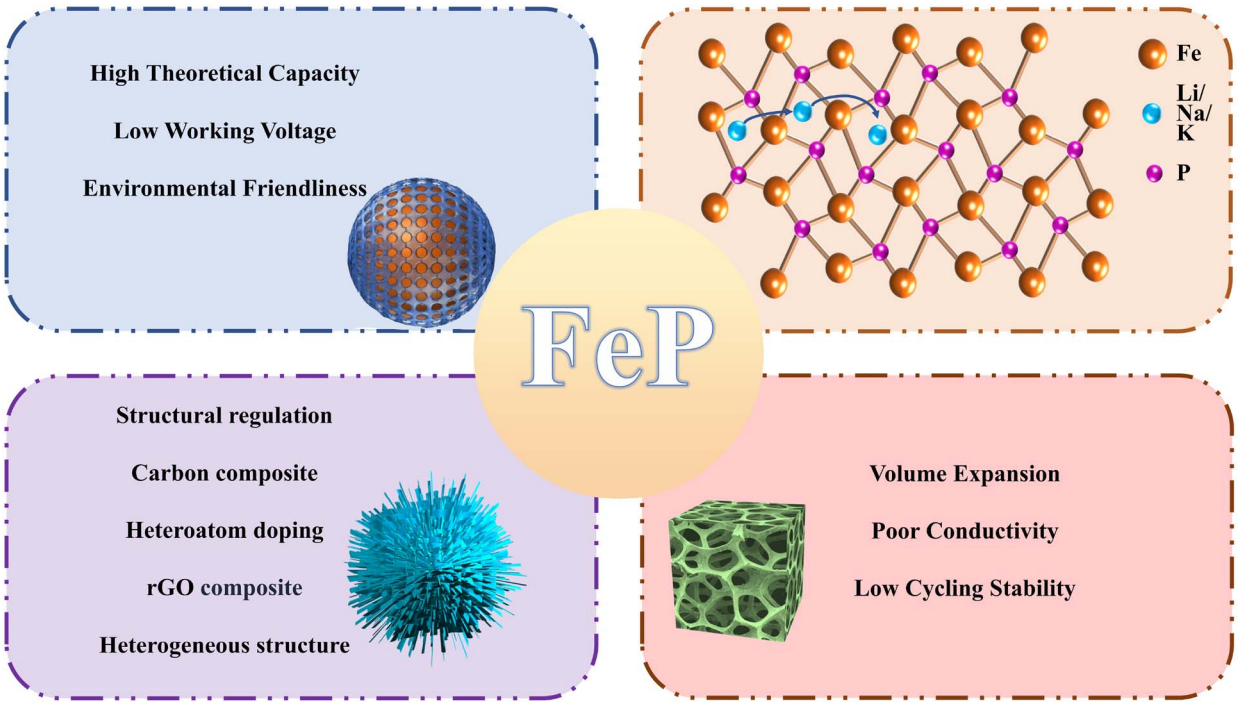

Fig. 1 Advantages, supercell of orthorhombic FeP, modification strategies and current challenges.

(SIBs) and potassium-ion batteries (PIBs), have been developed and extensively investigated due to the abundance of Na and K stores on Earth and the lower cost of use SIBs and PIBs share commonalities with LIBs in terms of electrochemical mechanisms, electrode materials, electrolytes, application areas, and environmental friendliness.[21–23] Nowadays, people have gained a deeper understanding of the research of AIBs, both in structural design, synthetic methods, and theoretical calculations. The cathode and anode are important components of AMIBs, which determine the electrode potential and energy density of the battery, so alkali metal ions ($Li^+/Na^+/K^+$) must be embedded and detached from the negative electrode material during the charging and discharging process. However, the lack of advanced anode materials limits the development of AMIBs. Commercial graphite anodes have a theoretical capacity of 372 mA h g^{-1} in lithium-ion batteries, making it difficult to meet future energy storage needs.[24–29] The theoretical capacity in Li-ion batteries is relatively low at 372 mA h g^{-1} because the ionic radii of Na^+ (1.02 Å) and K^+ (1.38 Å) are larger than that of Li^+ (0.76 Å), and they cannot accommodate the larger sizes of Na^+ and K^+.[30–32] This results in ion transport kinetics that are much inferior to those of LIBs, thus hindering the large-scale application and commercialisation of SIBs and PIBs. Therefore, the development and preparation of suitable Li^+, Na^+ and K^+ storage materials is crucial to drive the innovative development of energy storage battery technology.[33–37] Among many advanced anode materials, hard carbon, metal sulfides, metal oxides, and metal phosphides have been considered high-performance electrode materials for AMIBs, with the potential to replace traditional graphite. Hard carbon exhibits low charge/discharge voltage and high capacity; however, its initial coulombic efficiency is insufficient, which significantly limits its practical applicability.[38–40] Metal oxides and metal sulfides typically show high theoretical capacities, but during charge and discharge cycles, they often experience volume expansion and contraction, leading to structural degradation and, consequently, affecting cycle stability. Additionally, their low electrical conductivity necessitates the addition of conductive agents to improve conductivity; otherwise, the charge/discharge efficiency of the battery will be compromised.[41]

The selection of iron phosphide (FeP) as the anode material for alkali metal ion batteries over other metal phosphides is a strategic choice grounded in multiple advantageous characteristics. Firstly, FeP exhibits a relatively high theoretical capacity, which is crucial for achieving high energy density in batteries. This high capacity ensures that the battery can store and deliver a significant amount of energy, making it suitable for applications requiring long-lasting power supply. Secondly, the abundance and low cost of iron make FeP an economically viable option. In contrast, some other metal phosphides may involve more expensive metals, increasing the overall cost of battery production. Additionally, FeP demonstrates good electrochemical stability and structural integrity during charge–discharge cycles. Its ability to maintain structural stability under repeated cycling is essential for prolonging the battery's lifespan and ensuring consistent performance over time. Furthermore, recent research has shown that FeP can be effectively modified to enhance its conductivity and mitigate volume changes during cycling, further improving its electrochemical performance. These modifications, such as carbon coating or doping with other elements, have been successful in addressing some of the limitations associated with FeP, making it

Table 1 Differences in FeP anode materials in LIBs, SIBs and PIBs batteries

	LIBs	SIBs	PIBs
Specific capacity	Higher	Higher	Relatively low
Cyclic stability	Preferably	Excellent	Relatively low
Rate performance	Medium	Excellent	General
Ion diffusion and transport	Lithium-ion diffusion coefficient is moderate	Sodium-ion diffusion coefficient is higher, and its transport efficiency is better	Potassium-ion diffusion coefficient is relatively low, and its transport efficiency is average
Structural characteristics	The incorporation of FeP in lithium-ion batteries may facilitate the formation of a more uniform distribution of nanoparticles	The incorporation of FeP in sodium-ion batteries may lead to distinct aggregation states or crystal structures, such as those more favorable for sodium-ion intercalation	The structural characteristics of FeP in potassium-ion batteries remain less explored, and its structural adaptability may differ due to the larger ionic radius of K+, potentially resulting in unique phase configurations

a promising candidate for high-performance alkali metal ion batteries. In summary, the combination of high capacity, cost-effectiveness, and potential for performance enhancement through material modification makes FeP a preferred choice over other metal phosphides for use as anode materials in alkali metal ion batteries.[42–44] Therefore, it is of great scientific significance to develop high-performance FeP anode materials through rational and effective modification strategies to achieve stable and efficient electrochemical energy storage (Table 1).

This review presents a comprehensive review of the recent advancements in the modification of iron phosphide (FeP) as an anode material for alkali metal-ion batteries (AMIBs). The focus is deliberately placed on composite modification and the ensuing electrochemical pn enhancing the material's volumetric strain tolerance and performance, with particular emphasis on the significance of these strategies in action kinetics. We have delineated various modification strategies, including the composite with carbon materials, heteroatom doping, and the integration with reduced graphene oxide (rGO).

Carbon-based materials, such as carbon coating, porous carbon materials, and carbon nanotubes, are emphasized for their high specific surface area, stable electrochemical performance, and cost-effectiveness. The heteroatom doping with elements like N, P, Ni, and Cu has been shown to effectively increase the defect sites, porosity, interlayer conductivity, and overall electrical conductivity of carbonaceous materials. The composite with rGO is noted for its significant enhancement in the battery's conductivity, cycling stability, high-rate charge–discharge capability, and electrochemical performance.

These strategies are identified as effective avenues for the development of high-capacity anode materials for AMIBs. Therefore, elucidating their merits and progress is of substantial importance and necessity. Although several reviews have provided a broad overview of the developments in AMIBs, including advancements in cathode and anode materials, none have systematically focused on the breakthroughs of FeP as an anode material for AMIBs. Given the multitude of advantages that FeP anode materials possess, making them an ideal choice for electrochemical energy storage, this review synthesizes a wide array of literature concerning FeP anode materials, aspiring to contribute to the discourse within the field of electrochemical energy storage. In this work, we specifically concentrate on the composite modification of materials and an in-depth discussion of their electrochemical performance, offering a prospective outlook on their application in the realm of AMIB anode materials.

2 FeP anodes for lithium-ion batteries

Recently, transition metal phosphides have attracted considerable attention because of their abundance in natural resources and high theoretical capacities. In particular, iron phosphides (FeP), have been investigated as anode materials for LIBs owing to their high theoretical capacity of 926 mA h g^{-1}. However, the utilization of FeP (iron phosphide) as an anode material in lithium-ion batteries is associated with several significant limitations. These include low conductivity, electrode material chalking, and a rapid reduction in battery capacity, in addition to unstable electrochemical performance. To enhance their electrochemical characteristics, FeP nanostructures are typically designed or combined with carbon to augment electrical conductivity and mitigate volume expansion. In this section, we focus on the structural modulation of FeP anode materials, composites with carbonaceous materials, and the construction of heterostructures.

Lithiation was confirmed as an insertion/conversion type reaction as follows:

$$FeP + xLi^+ + xe^- \leftrightarrow Li_xFeP\ (x = 0–3)$$

$$Li_xFeP + (3 - x)Li^+ + (3 - x)e^- \leftrightarrow Li_3P + Fe$$

2.1 FeP with structural regulation

Veluri *et al.* successfully prepared iron phosphide (FeP) from iron oxide (Fe_2O_3) using a scalable two-step approach.[45] When used as anode materials for lithium-ion batteries, they exhibit good electrochemical properties. In comparison to lithium, the electrochemical performance exhibits a capacity retention of 53.7% of the second discharge capacity (622 mA h g^{-1}) after 50 cycles using a CMC binder, which incorporates both the insertion and

conversion reactions. Yan *et al.* conducted density functional theory (DFT) calculations and designed MOF-derived porous FeP nanorods modified by abundant P vacancies (denoted as V-FeP) *via* a simplified approach, guided by the principles of density functional theory (Fig. 2a).[46] When used as anode materials for lithium-ion batteries, Fig. 2b and c shows they exhibit good electrochemical properties (impressive specific capacity (1228.3 mA h g^{-1} at 0.1 A g^{-1} after 120 cycles)) and Fig. 2d shows the long-cyclic performance (590.7 mA h g^{-1} at 2.0 A g^{-1} after 1000 cycles). The presence of a multitude of P vacancies served as charge carriers, enhancing conductivity and furnishing a plethora of active sites for lithium storage. Furthermore, the even distribution of the conductive carbon network coating nanoparticles reduced the diffusion distance of Li ions, alleviated the volume change, impeded electrode pulverization, and enhanced the migration rate of Li ions in the internal structure.

Murali *et al.* present a straightforward, vapor-phase conversion of prominent metal oxalates into metal phosphide nanostructures (FeP), with a particular focus on their potential application in lithium-ion batteries.[47] When employed as anode materials for lithium-ion batteries, they demonstrate favorable electrochemical characteristics. The cycle life assessment of FeP revealed a reversible storage capacity of 387 mA h g^{-1} for LIB at a current density of 250 mA g^{-1} over 250 cycles. In general, the FeP electrode demonstrated favorable performance as an anode for alkali ions, exhibiting higher capacity, rate capability, higher coulombic efficiency, stable cycling, and enhanced kinetics. Liu *et al.* employed a magnetic field-assisted and templated approach to encapsulate multiple FeP nanospheres inside a FeP nanotube, thereby forming a nanosphere-in-nanotube yolk–shell (NNYS) structure (Fig. 2e).[48] When employed as anode materials for lithium-ion batteries, they demonstrate favorable electrochemical characteristics. Following 100 cycles at 0.5 A g^{-1} (Fig. 2h), the NNYS FeP exhibits a capacity of 661 mA h g^{-1} and a coulombic efficiency of 99.8%. With this method, the prepared NNYS FeP anode is optimal, including a stable capacity after 1000 cycles are shown in Fig. 2f and g, low and high-temperature tolerance, and reversible rate performance. Kundu *et al.* used thermal oxidation and phosphorylation of FeOOH nanorods to make Fe_2O_3 and FeP nanotubes, they inherited the same size and shape as the original nanorods.[49] Moreover, after 1200 cycles at a high current density of 1000 mA g^{-1}, the specific capacity of FeP NTs was found to be 1897 mA h g^{-1}. Moreover, when cycling at a higher current density of 3000 mA g^{-1}, the specific capacities remained at 603.4 mA h g^{-1} for FeP NTs after 1400 cycles, which is noteworthy for conversion-type anode materials. Boyanov *et al.* determined that a reversible two-stage insertion/conversion process was responsible for the encouraging performance of the FeP electrode.[50] The reversible insertion process resulted in notable capacity retention, with 300 mA h g^{-1} and 1900 mA h cm^{-3} retained after 100 cycles.

2.2 FeP with carbon composite

However, the low electronic conductivity and substantial volume expansion of the FeP anode during charging and

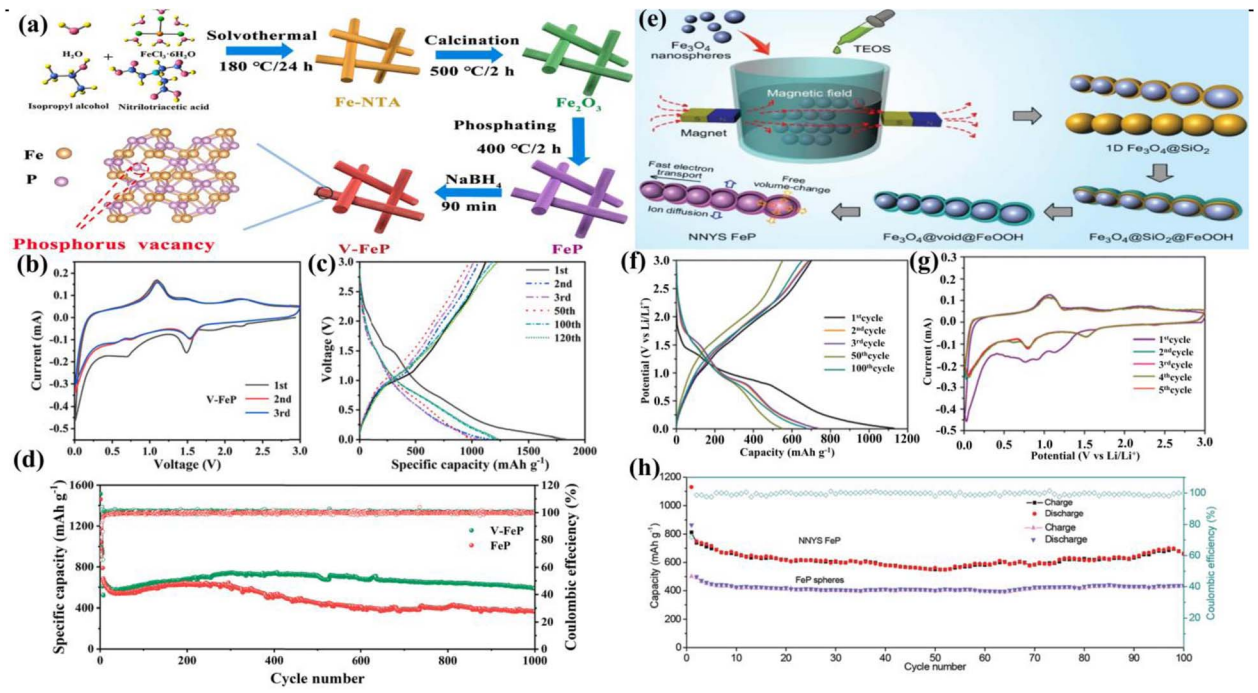

Fig. 2 (a) Schematic illustration of the preparation of V-FeP nanorods. (b) CV curves for the first three cycles of V-FeP nanorods at 0.2 mV s^{-1}. (c) Charge/discharge curves of the V-FeP nanorods at the 1st, 2nd, 3rd, 50th, 100th, and 120th at 0.1 A g^{-1}. (d) Long-cyclic performance of V-FeP and FeP nanorods at 2.0 A g^{-1}. (e) The preparation process of the NNYS FeP through a magnetic field-assisted and templated approach. (f) Charge–discharge curves of the NNYS FeP at 0.5 A g^{-1}. (g) First-five CV curves at 0.1 mV s^{-1}. (h) Capacities of NNYS FeP and FeP nanospheres at 0.5 A g^{-1}.

discharging frequently result in suboptimal performance. One efficient solution is to embed FeP in a carbon matrix to create a composite. The carbon matrix can effectively mitigate the volume expansion of FeP and facilitate the formation of ion channels, thereby enhancing the electrical conductivity. Representative carbon materials include amorphous carbon, CNF, CNT, and rGO. Gao *et al.* have developed porous FeP@C networks through a one-step calcination process, utilizing ferric nitrate and phytic acid as precursors for FeP, along with thiourea and melamine as nitrogen and sulfur precursors (Fig. 3a).[51] The resulting FeP@C anode materials exhibit excellent rate capability and cycling stability, achieving a reversible capacity of 293.0 mA h g^{-1} at 4 A g^{-1} after 1000 cycles (Fig. 3d). Even at an ultrahigh current density of 6 A g^{-1}, they maintain a reversible capacity of 218.3 mA h g^{-1}. This porous architecture significantly enhances electrolyte penetration and shortens the transfer length of Li^+ ions. The carbon matrix not only provides structural support but also enhances the electrical conductivity, contributing to the overall performance of the FeP@C composite. Additionally, the conductive carbon coating on FeP effectively mitigates volume changes during cycling and boosts electronic conductivity. Due to their unique structure, Fig. 3b and c displays the FeP@C networks demonstrate competitive rate performance and cycling stability, coupled with a substantial reversible capacity. Zhang *et al.* have developed Fe_xP/C core–shell nanocubes with a large internal void space, synthesized using Prussian blue (PB) as a precursor and a low-temperature phosphidation strategy.[52] The distinctive core–shell structure of a substantial void inner space contributed to the favorable electric performance of the FexP/C, which demonstrated a reversible capacity of 665 mA h g^{-1} following 200 cycles at 100 mA g^{-1}. The excellent performance of FexP/C as an anode material for lithium-ion batteries can be attributed to the fact that the FexP/C nanocubes possess sufficient inner void space, which can accommodate the considerable volume expansion of the internal Fe_xP nanoparticles during the Li^+ intercalation and deintercalation process. Furthermore, the carbon shell contributes to the high performance by providing a conductive network and mitigating volume expansion during the Li^+ intercalation and deintercalation process and the carbon shell can enhance the conductivity of the electrodes, which is beneficial for the transportation of Li^+. Xu *et al.* successfully fabricated carbon-encapsulated FeP nanoparticles with a 3D porous hierarchical structure *via* a general MOF-derived gas phosphidation strategy.[53] When the FeP@C anode exhibits a high reversible capacity of 700 mA h g^{-1} at 0.1 A g^{-1} over 180 cycles for Li-ion batteries. The exceptional rate capability and ultrastable cycling performance can be attributed to the 3D porous carbon-encapsulated FeP nanoparticles, which serve to enhance structural stability, expand active surface areas, improve electrical conductivity, accelerate ion/electron transport, and provide ample void space to alleviate volume expansion during repeated cycling. Zhou *et al.* constructed a high-capacity, self-adaptive FeP@C nanocage with fast kinetics through a self-

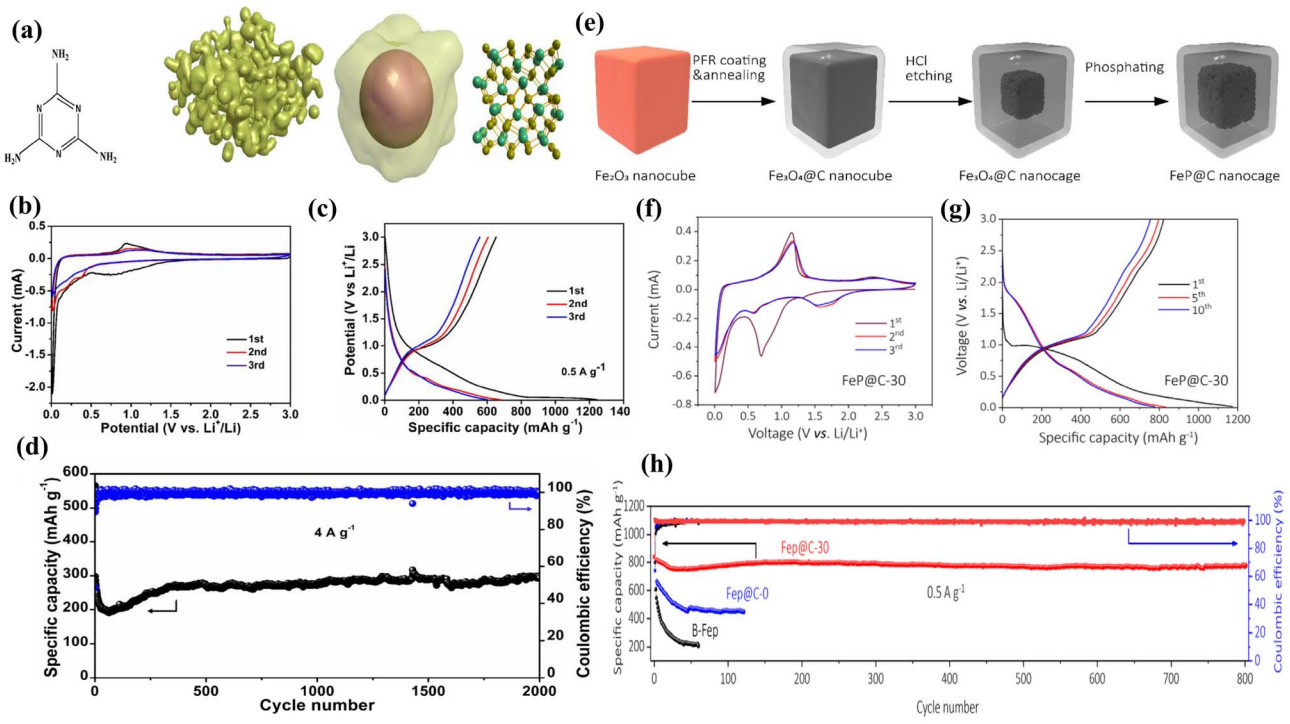

Fig. 3 (a) Schematic illustration of the synthesis process of FeP@C frameworks. (b) CV curves in the initial three cycles at the scan rate of 0.2 mV s^{-1} between 0.01 and 3 V. (c) Charge/discharge profiles in the potential window of 0.01–3 V at 0.5 A g^{-1}. (d) Cycling performance of the FeP@C electrode at 4 A g^{-1}. (e) Schematic illustration of the construction of FeP@C nanocages. (f) CV curves of FeP@C nanocages for the first three cycles at the scan rate of 0.2 mV s^{-1}. (g) Charge/discharge curves for the 1st, 5th, and 10th cycles at 0.2 A g^{-1}. (h) Cycling performance of B-FeP, FeP@C-0, and FeP@C-30 at 0.5 A g^{-1}.

template method and an etching process by tuning the antihunt interface (Fig. 3e).[54] The assembled Li/FeP@C half battery. The material exhibits a high reversible capacity, reaching approximately 900 mA h g^{-1} at 0.2 A g^{-1}, and demonstrates long-term stability, retaining approximately 680 mA h g^{-1} at 0.5 A g^{-1} over 800 cycles (Fig. 3h). The excellent electrochemical characteristics as shown in Fig. 3f and g are ascribed to the FeP@C nanocages, which exhibit a high surface area, thereby enhancing the number of reactive sites for the transfer of electrons and ions. Furthermore, the typical intermediate cushion spaces provide an electrochemical environment that is resistant to accommodate the significant pulverization of the inner FeP nanoparticle during lithiation and delithium, while the outer mesoporous carbon facilitates the formation of a stable SEI layer. Conformally carbon-coated FeP nanoplates with porous features are synthesized through the integration of three simple approaches. The carbon coating on FeP nanospheres effectively mitigates volume expansion during charge–discharge cycles and provides a conductive network that enhances the electrode's electrical conductivity and structural stability. These include the hydrothermal growth of Fe_2O_3 nanoplates, the introduction of a conformal carbon coating at a specific spatial location, and the conversion of an intermediary into FeP *via* a low-temperature phosphidation strategy.[55] The rationally designed material functions as an anode for lithium-ion batteries (LIBs) and exhibits an exceptional electrochemical performance, characterized by a high reversible capability (720 milliampere hours per gram at a current density of 200 milliampere per gram), excellent cycling stability (the material exhibits an impressive capacity of 10 milliampere-hours per gram at a high current density of 500 milliampere per gram over 400 cycles), with minimal capacity loss. Additionally, it demonstrates remarkable rate capability, reaching 347 milliampere-hours per gram at 5000 milliampere per gram. The exceptional lithium-ion storage capabilities of the FeP@C nanoplates can be attributed to three key factors: a reduced energy barrier for the lithium storage reaction, shortened electronic and ionic transfer paths, and a physical buffering effect resulting from the strategic integration of phosphide-based species, plate-like nanostructure, and conformal carbon surface modification.

Significantly enhancing the electrochemical performance of FeP anode materials through carbon coating has been well demonstrated in previous studies. Its integration with carbon nanomaterials opens up new possibilities for further optimization of structural and interfacial properties. This section will focus on the combining of carbon-coated FeP anode materials with carbon nanomaterials. Li *et al.* employed ball milling-pyrolysis to encapsulate monodisperse FeP nanoparticles with a particle size of only 8 nm in carbon.[56] As anode material, it exhibits a specific capacity of approximately 500 mA h g^{-1} at a current density of 500 mA g^{-1} following 600 cycles. The incorporation of FeP nanoparticles into the conductive carbon layer with a monodispersed nature not only increases the contact areas between the two materials but also reduces the average stress generated in the materials during the discharge/charge process. This is beneficial for maintaining the structural integrity of the material during cycling. Zhang *et al.* synthesized shuttle-like hollow and porous carbon-coated FeP (FeP@C) structures from Fe-based metal–organic frameworks (MOFs) MIL-88. These structures were then employed as anodes for lithium-ion batteries (LIBs).[57] Consequently, lithium-ion batteries comprising FeP@C as the anode material exhibit a considerable maximum lithium storage capacity of 902.4 mA h g^{-1} at 0.1 A g^{-1} for 100 cycles. Furthermore, the batteries exhibit superior rate capability, with a reversible capacity of 416 mA h g^{-1} at 5.0 A g^{-1}, and long-life cycling performance, with 3000 cycles at 5.0 A g^{-1}. The carbon coating on FeP nanospheres effectively mitigates volume expansion during charge–discharge cycles and provides a conductive network that enhances the electrode's electrical conductivity and structural stability. Wang *et al.* employed an effective synthetic strategy, combining the etching-in-boxes and phosphidation-in-boxes approaches, to design and construct yolk–shell FeP@carbon (FeP@C) nanobox composites with void space (Fig. 4a).[58] When employed as an anode material for lithium-ion batteries, the as-built FeP@C nanoboxes exhibit an excellent rate capability, with high specific capacities of 495.9 and 220.8 mA h g^{-1} at 1.0 and 10.0 A g^{-1}, respectively. Because of these unique structural merits, the as-built FeP@C nanobox electrode manifests superb lithium storage properties in terms of high specific capacity (Fig. 4b), outstanding rate capability (Fig. 4c), and long cycling stability (Fig. 4d). Yang *et al.* synthesized uniform yolk–shell FeP@C nanoboxes (FeP@CNBs), in which the inner FeP nanoparticles are completely protected by a thin and self-supported carbon shell. This was achieved through a phosphidation process utilizing yolk–shell Fe_2O_3@CNBs as a precursor.[59] The as-synthesized FeP@CNBs electrode has demonstrated a high reversible capacity of 609 mA h g^{-1} at 100 mA g^{-1} for lithium-ion batteries (LIBs), respectively. Furthermore, the electrode has demonstrated remarkable rate performance (380 mA h g^{-1} at 2 A g^{-1}) and an ultralong cycling life (476 mA h g^{-1} after 400 cycles at 500 mA g^{-1}) in LIBs. The enhanced electrochemical performance of the composite is attributable to its unique structure, wherein the carbon shell functions as a barrier, impeding the aggregation of FeP nanoparticles and thereby augmenting the electrical conductivity of the composite. Moreover, the void space between the carbon shell and FeP facilitates volume expansion during the charging and discharging processes, thus mitigating potential damage to the electrode microstructure. Following modification, the coulombic efficiency exhibited a notable increase, rising from approximately 50% to 87%. Jiang *et al.* have successfully synthesized composites consisting of pure-phase FeP nanorods *in situ* coated with carbon shells (referred to as nanorod-FeP@C composites).[60] These composites were obtained by adjusting the molecular ratio of $Fe(C_5H_5)_2$ and PPh_3 precursors in a sealed quartz tube, followed by heating at 390 °C for 10 hours. Comprehensive characterizations and determinations confirmed the successful synthesis. In terms of electrochemical performance, these nanorod-FeP@C composites initially deliver a specific capacity of 330 mA h g^{-1}, which improves to 480 mA h g^{-1} after 200 cycles at a current density of 30 mA g^{-1}. Electrochemical investigations reveal that while the capacity of

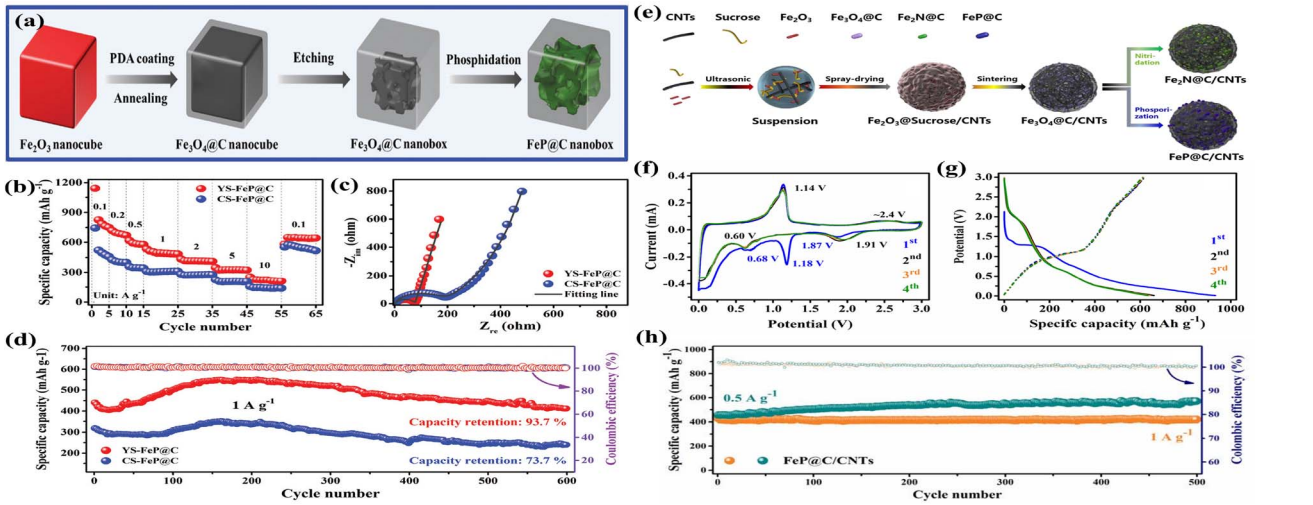

Fig. 4 (a) Schematic illustration of the synthesis process for the FeP@C nanoboxes. (b) Rate performances of YS-FeP@C and CS-FeP@C electrodes. (c) Nyquist plots of YS-FeP@C and CS-FeP@C electrodes. (d) Cycling performance of YS-FeP@C and CS-FeP@C electrodes at 1.0 A g^{-1}. (e) The fabrication mechanism of the hierarchical polycystic microsphere anode mate. (f) CV curves at a scan rate of 0.1 mV s^{-1} (g) Galvanostatic discharge/charge profiles at a current density of 0.1 A g^{-1}. (h) Cycle stability of FeP@C/CNTs composites at 0.5 A g^{-1} and 1 A g^{-1} as well as their corresponding efficiency.

the FeP phases in the composites is lower than their theoretical capacity, the carbon shell exhibits a high capacity. Additionally, the presence of the carbon shell contributes to the composites' excellent cyclic stability. Wang *et al.* report the development of a novel one-dimensional hierarchical material, comprising carbon-coated mini hollow FeP nanoparticles homogeneously encapsulated within porous carbon nanofibers (denoted as M-FeP@C).[61] This material was synthesized through a low-temperature phosphidation method. When utilized as an anode material for lithium-ion batteries (LIBs), the M-FeP@C hybrid nanofibers exhibit a high reversible capacity of 806 mA h g^{-1} at 0.25 A g^{-1} after 100 cycles. The exceptional electrochemical performance of the M-FeP@C hybrid nanofibers for both lithium and sodium storage are attributed to the advantageous embedding architecture. This architecture, featuring mini hollow FeP nanoparticles and a double carbon layer scaffold, provides a continuous conducting framework and nanoporous channels for efficient ion and electron diffusion and transport. Additionally, it offers sufficient voids to mitigate volume changes during cycling. Yang *et al.* demonstrate the successful development of a high-capacity anode for lithium-ion batteries (LIBs) by confining FeP nanoparticles within porous and electrically conductive carbon nanofibers (NFs).[62] This was achieved through a combination of electrospinning, carbonization, oxidation, and phosphidation procedures. When utilized as an anode material for LIBs, this innovative structure delivers an impressive specific capacity of approximately 1160 mA h g^{-1}. Additionally, it exhibits excellent stability, maintaining performance over 300 low-rate cycles and 1000 high-rate cycles. Hou *et al.* have successfully prepared carbon-coated FeP nanorods (FeP@C-NR) grown on carbon nanotubes (CNTs), referred to as CNTs⊥FeP@C-NR, *via* a straightforward two-step method.[63] When utilized as an anode material for lithium-ion batteries (LIBs), this material demonstrates remarkable cycling stability, achieving a specific capacity of 1129 mA h g^{-1} after 300 cycles at 0.5 A g^{-1} and 1126 mA h g^{-1} after 300 cycles at 1 A g^{-1}. The excellent electrochemical performance is attributed to the unique structural design of the carbon nanotube-coated FeP@C-NR, which provides superior electrical conductivity, structural stability, and pseudocapacitance-enhanced ultrafast electrochemical kinetics. Jing *et al.* reported a novel approach combining spray-drying and chemical conversion strategies to successfully design hierarchical polycystic FeP@C/CNTs hybrids (Fig. 4e).[64] Fig. 4h shows the FeP@C/CNTs electrode demonstrates a reversible capacity of 587 mA h g^{-1} after 500 cycles at a current density of 0.5 A g^{-1}. Even at a high rate of 5 A g^{-1}, it exhibits a reversible capacity as high as 232 mA h g^{-1}. Fig. 4f and g shows that excellent electrochemical performance is attributed to several factors: (1) the nanosized materials efficiently improve ion kinetics by shortening the transport distance of Li^+. (2) The amorphous carbon coating and high-conductivity CNTs embedded into the porous microspheres construct a three-dimensional continuous conductive network for electrons. (3) The amorphous carbon and CNTs form a protective cage that effectively buffers the significant volume expansion during the conversion reaction while ensuring intimate contact between the anode materials and the conducting carbon network. Xu *et al.* successfully synthesized self-supported FeP@C nanotube arrays on flexible carbon fabric *via* facile template-based deposition and phosphorization routes.[65] When utilized as an anode material for lithium-ion batteries (LIBs), these FeP@C nanotube arrays achieve high reversible capacities of 945 mA h g^{-1} at 0.1 A g^{-1} and 761.92 mA h g^{-1} at 0.8 A g^{-1} (1.73 and 1.39 mA h cm^{-2} at 0.18 and 1.46 mA cm^{-2}, respectively). The flexible FeP@C/CF electrode also retains a capacity of 718 mA h g^{-1} (1.31 mA h cm^{-2}) over 670 cycles at 0.5 A g^{-1} (0.92 mA cm^{-2}) and 500 mA h g^{-1} (0.92 mA h cm^{-2}) over 1100 cycles at 1.5 A g^{-1} (2.75 mA cm^{-2}). The superior rate capability and ultra-stable cycling performance

of the self-supported FeP@C electrode can be attributed to the structure of the carbon-coated nanotube arrays, which enlarge the active surface areas and enhance the overall electrochemical performance.

2.2.1 FeP with heteroatom doping. Lin *et al.* developed a novel Cu-doped FeP@C through a synergistic approach combining metal doping and *in situ* carbon encapsulation.[66] The optimized Cu-FeP@C anode exhibits a high specific capacity (920 mA h g^{-1} at 0.05 A g^{-1}), excellent rate performance (345 mA h g^{-1} at 5 A g^{-1}), and long cycle stability (340 mA h g^{-1} at 2 A g^{-1} after 600 cycles). In comparison to previously documented FeP-based anodes, the Cu-doped FeP@C demonstrates an exemplary electrochemical performance. Three-dimensional carbon frameworks expand the volume and prevent nanoparticle accumulation. They provide conductive routes and channels for electrolytes. Furthermore, Cu doping regulates the charge density distribution in the crystal and enriches the surface-active sites of the electrode, thereby accelerating electron mobility and facilitating charge storage. Zhang *et al.* designed and prepared FeP/NPCS nanocomposites *via* a one-step calcination process, utilizing phytic acid as a phosphorus and metal ion chelator and melamine as an N and carbon source.[67] When employed as an anode material, FeP/NPCS exhibits remarkable multiplicative capacities of 764 and 385 mA h g^{-1} at 0.1 A g^{-1} and 2.0 A g^{-1} current densities, respectively. Furthermore, the intimate relationship between FeP and carbon nanosheets also endows it with excellent long-term activity and durable cycling stability, with a retention of over 134% (831.2 mA h g^{-1}) at a current density of 0.5 A g^{-1}. More importantly, the materials synthesized by this method have the potential for use in a variety of applications, including supercapacitors and electrochemical catalysis. Zheng *et al.* have successfully developed an excellent LIBs anode candidate of 3D flake-CNs-like configuration *via* a delicate architectural design and a facile synthesis approach.[68] This configuration consists of amorphous FeP nanoparticles encapsulated in ultrathin 3D interconnected P-doped porous CNs. The FeP@CNs anode displays a high reversible capacity of 837 mA h g^{-1} after 300 cycles at 0.2 A g^{-1} and an excellent rate capability of 403 mA h g^{-1} at 16 A g^{-1}. Furthermore, it exhibits remarkable cycling stability, retaining 98% of its capacity even after 2500 cycles at 4 A g^{-1}. The FeP@CNs electrodes demonstrate exceptional lithium storage performance, exhibiting high reversible capacity, remarkable rate capability, and ultralong cycling life. Li *et al.* employed a solvothermal method and a subsequent phosphation process to develop a novel 3D hierarchical flower-like FeP coated with nitrogen-doped carbon assembled from porous nanosheets (FeP@N, C hybrid).[69] Moreover, the 3D hierarchical flower-like FeP@N, C hybrid exhibits remarkable cyclic stability (569 mA h g^{-1} at a current density of 500 mA g^{-1} for the 300th cycle) and rate performance (331.94 mA h g^{-1} at a high current density of 5 A g^{-1}) for lithium-ion batteries (LIBs). Furthermore, the flower-like FeP@N, C hybrid displays a substantial surface area, thereby enhancing the contact area between the electrode and the electrolyte and providing a considerable buffer space. In consequence, the flower-like FeP@N, C hybrid exhibits satisfactory electrochemical functionality. Yang *et al.* have developed a hierarchically porous iron phosphide nanospindle structure with nitrogen–phosphorus-codoped carbon coatings (FeP@NPC) *via* a two-step process involving hydrothermal synthesis and subsequent phosphating treatment.[70] The as-prepared hierarchical FeP@NPC compound exhibits high specific capacity, excellent rate performance, and remarkable cycling stability. The porous nanospindle FeP is capable of efficiently realizing capacity improvement and rapid ion transportation during the long-cycling process. The FeP@NPC anode exhibits a notable specific capacity of 1100 mA h g^{-1} after 200 cycles at 0.2 A g^{-1}, a commendable ranking rate performance. The capacity is approximately 600 mA h g^{-1} at 5 A g^{-1}, and a reversible long cycling capacity of 951.7 mA h g^{-1} is observed after 800 cycles at 1 A g^{-1}. Wang *et al.* synthesized a coral-like FeP composite with FeP nanoparticles anchored and dispersed on a nitrogen-doped three-dimensional carbon framework (FeP@NC) through an *in situ* phosphating/carbonization process of polymer precursors (6h-FeP@NC-1).[71] The anode material, 6h-FeP@NC-1, exhibited discharge capacities of 704.6, 604.9, 541.1, 484.8, 434.3, 362.2, 305.9, and 238.4 mA h g^{-1} at current densities of 0.1, 0.2, 0.5, 1, 2, 5, 10, and 20 A g^{-1}, respectively. Furthermore, the 6h-FeP@NC-1 electrode exhibited a discharge capacity of 269.6 mA h g^{-1} at 5 A g^{-1}. The electrode demonstrated a capacity retention of 90.3% at 10 A g^{-1} over 5000 cycles and a high reversible capacity of 649.7 mA h g^{-1} after 300 cycles at 0.1 A g^{-1}. Furthermore, it exhibited excellent stability over 2500 cycles, with a capacity retention of A g^{-1}. This evidence indicates that, in addition to its notable rate capability, the FeP@NC composites exhibit remarkable cycling stability. Wang *et al.* report an amine-functionalized MOF-derived strategy on morphological and interfacial modulation for the synthesis of porous structures with strongly coupled FeP nanocrystals and N-doped carbon frameworks, which were anchored onto CC firmly (denoted as FeP/NC@CC).[72] When used as a binder-free flexible anode for LIBs, the three-dimensional (3D) hierarchical FeP/NC@CC architecture delivers a reversible areal capacity of 5.8 mA h cm^{-2} at 0.15 mA cm^{-2} with high ICE up to 80.5% and excellent rate capability up to 6.0 mA cm^{-2} with a reversible capacity of 2.0 mA h cm^{-2}. FeP/NC@CC can be directly applied as a binder-free flexible electrode for LIBs and has excellent mechanical flexibility, high ICE, and areal capacitance. Yan *et al.* prepared a Ni-doped Ni-FeP@carbon (Ni-FeP@C) core–shell structure using a solvothermal method and phosphating process. This material has been designed as an anode for lithium-ion batteries (LIBs).[73] When employed as an anode material for lithium-ion batteries, the Ni-FeP@C composite exhibited remarkable specific capacity (855.7 mA h g^{-1} at 0.1 A g^{-1}) and exceptional long-cyclic performance (488 mA h g^{-1} after 1000 cycles at 2.0 A g^{-1}). This specific structure offered plentiful benefits: (i) Ni doping adjusted the electronic structure of FeP and improved its electrical conductivity, facilitating the diffusion rate of Li ions; (ii) carbon shell could relieve volume expansion during discharge/charge possess, preventing pulverization and aggregation, and strengthing the structure of stability. Zhang *et al.* have successfully prepared P-doped onion-like carbon layers coated

FeP (FeP@(P, OLC)) nanoparticles *via* a one-pot process involving arc discharging of Fe–P powers under a gas mixture of argon, hydrogen, and ethanol. This innovative approach has been designed to achieve excellent performance as an anode in LIBs.[74] The FeP@(P, OLC) core–shell structured nanoparticles, when employed as anode materials, exhibited a high initial capacity (1306 mA h g^{-1} at 0.1 A g^{-1}) and an initial CE value of 79.8%, which was of a high standard. Furthermore, they demonstrated a long lifespan (915 mA h g^{-1} at 500 cycles at 0.1 A g^{-1}) and excellent multiplicative performance (average capacity of 379 and 107 mA h g^{-1} at 8.0 and 10.0 A g^{-1}, respectively). 237 mA h g^{-1} at 8.0 and 10.0 A g^{-1}, respectively. The favorable electrochemical performance can be attributed to the distinctive structure of the composite, which has the effect of alleviating the aggregation of FeP nanoparticles, offering effective channels for electrons and ions, and buffering the volume change of FeP nanoparticles, which are induced by the P-doped OLC shells. This results in the superior lithium storage performance of FeP@(P, OLC) core–shell structured nanoparticles. Lin *et al.* have successfully fabricated an iron phosphide (FeP) nanorod and phosphorus-doped carbon (P-C) composite (nanorod-FeP@P-C) through a two-step strategy.[75] The utilization of nanorod-FeP@P-C composites as anodes has been demonstrated to result in a Li-ion storage capacity of 714 mA h g^{-1} at a current density of 100 mA g^{-1}. Following 800 cycles at a current density of 2 A g^{-1}, a remaining capacity of 625 mA h g^{-1} was observed. Upon increasing the current density to 5 A g^{-1}, a capacity of 420 mA h g^{-1} was retained, indicative of superior rate capability. Li *et al.* successfully fabricated a FeP anode with a uniform carbon coating using a facial chemical coordination method followed by heat treatment (Fig. 5a).[76] When assembled into LICs with commercial AC, the energy density reaches 84.6 W h kg^{-1} at 0.05 A g^{-1} and maintains 81.5 W h kg^{-1} at 1.0 A g^{-1}, with a retention ratio of 91.8% after 5000 cycles (Fig. 5d). In this study, Li *et al.* employed the chelate metal–phosphorus interaction *via* coordination to efficiently fabricate high-capacity FeP anodes. The results demonstrated that the synthesized nanorod-like FeP was enveloped by an amorphous carbon layer, characterized by a porous and nitrogen-doped structure. This configuration achieved an impressive specific surface area of 412.86 m^2 g^{-1}, exhibiting a mesoporous distribution. Additionally, a carbon coating layer with a thickness of 7.5 nm was observed. The presence of the carbon buffer layer, along with the carbon coating and nitrogen-rich porous structure, Fig. 5b and c displays the significantly enhanced electrochemical kinetics of the FeP anode. Yu *et al.* have successfully synthesized biconical-nanorod-like Co-doped FeP confined by phosphorus-doped carbon (Co-doped FeP@P-C) derived from metal–organic frameworks (MOFs) through a hydrothermal process followed by a phosphorization strategy (Fig. 5e).[77] This unique biconical-nanorod-like architecture significantly enhances the material's contact area with the electrolyte, thereby accelerating electrolyte penetration and promoting efficient ion and electron transport. Moreover, the intentional doping of cobalt ions is designed to modify the electronic structure of the FeP material, further boosting charge transfer kinetics. The phosphorus-doped carbon layer, derived from MOFs, not only enhances electrical conductivity but also maintains structural integrity by preventing material collapse and agglomeration. As demonstrated in Fig. 5f and g, the FeP@P-C anode exhibits exceptional electrochemical properties. As a result of these superior characteristics, the Co-doped FeP@P-C anode exhibits a high specific capacity of 784 mA h g^{-1} at 0.2 A g^{-1} and demonstrates outstanding long-

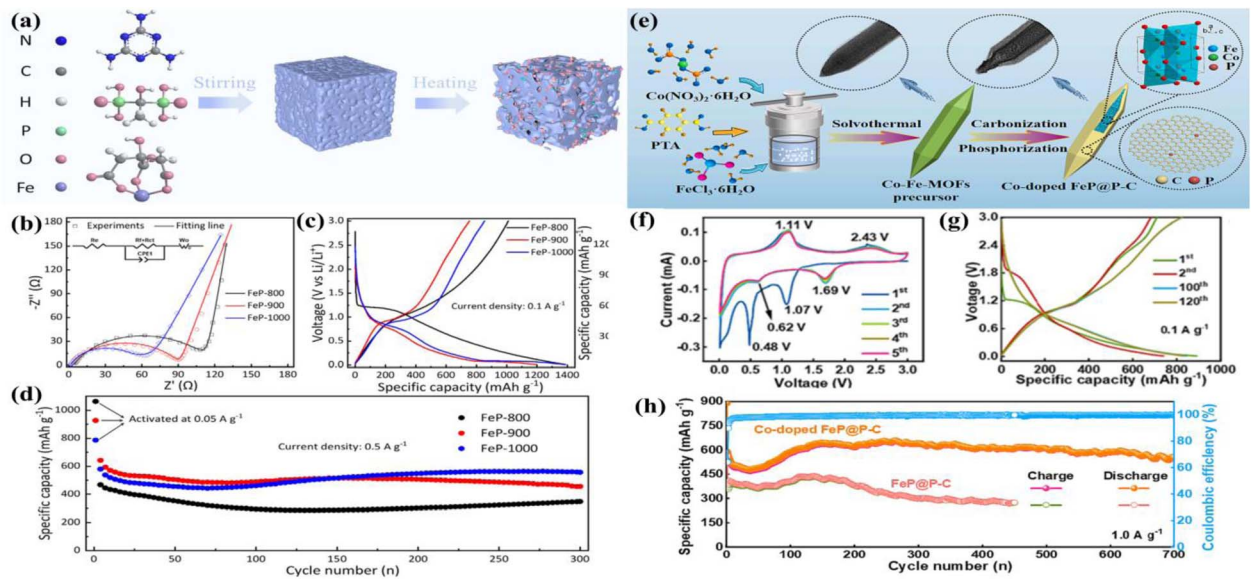

Fig. 5 (a) Schematic route of FeP samples. (b) EIS test. (c) First three charge–discharge profiles of FeP derivatives at 0.1 A g^{-1}. (d) Long-term cycling stability test at 0.5 A g^{-1}. (e) Schematic illustration of the fabrication process and structure of biconical-nanorods-like Co-doped FeP@P-C architecture. (f) CV curves at a scan rate of 0.2 mV s^{-1}. (g) Charge–discharge curves at 0.1 A g^{-1}. (h) Cycling performances at 1.0 A g^{-1} current densities.

term cycling stability, retaining 555.6 mA h g^{-1} at 1 A g^{-1} after 700 cycles (Fig. 5h), making it a promising candidate for lithium-ion batteries (LIBs).

2.2.2 FeP with rGO composites. Hou *et al.* have successfully prepared a hierarchical G⊥FP@C-NA nanocomposite, consisting of carbon-coated FeP nanorod arrays (FP@C-NA) grown vertically on a 2D reduced graphene oxide (G) network, *via* a simple solution reaction followed by a phosphidation treatment.[78] The G⊥FP@C-NA exhibits a high lithium storage capacity (1106 mA h g^{-1} at 50 mA g^{-1}), outstanding rate capability (565 mA h g^{-1} at 5000 mA g^{-1}), and long-term stability. The material demonstrated excellent cycling stability, retaining a capacity of 1009 mA h g^{-1} at 500 mA g^{-1} after 500 cycles and 310 mA h g^{-1} at 2000 mA g^{-1} after 2000 cycles when employed as an anode material for LIBs. The favorable electrochemical performance is attributed to the spaces between FP@C-NA in G⊥FP@C-NA, which provide sufficient buffer spaces for the considerable volume expansion that occurs during the lithiation process. And enhances the cycling stability of the materials. Concurrently, the interstitial spaces between the FP@C-NA facilitate the infiltration of the electrolyte and effectively accelerate the electrochemical kinetics, thereby enabling the prepared G⊥FP@C-NA to exhibit a pseudo-capacitance-boosted ultrafast lithium storage performance. Li *et al.* successfully developed an efficient hydrothermal and carbonization process to encapsulate capsule-like FeP nanoparticles in a nitrogen-doped carbon layer (FeP@NC). At the same time, FeP@NC was anchored to the sheet-like rGO surface, resulting in a marvelous three-dimensional (3D) structure, FeP@NC@rGO (FPCG) (Fig. 6a).[79] As an anode for LIBs, the FPCG electrode materials exhibit high reversible capacities of 927 mA h g^{-1} at 0.2C after 170 cycles, an excellent rate capacity of 486 mA h g^{-1} at 5C in Fig. 5b, c and 6d shows the exceptional durability (500 cycles, 863 mA h g^{-1} at 0.5C, 97.7% capacity retention). The electrochemical performance is greatly improved after FeP is combined with rGO and N-doped carbon, which is due to the diffusion path of Li^+ being shortened by the nanoscale of FeP, the 3D conductive network improving electrical conductivity, and the incorporation of N enhancing the insertion and removal of Li^+. Gao *et al.* successfully developed a double carbon-coated FeP composite (FeP@NC@rGO), which was fabricated *in situ via* the phosphorization process of the prepared Prussian blue@graphene oxide (PB@GO) precursor.[80] When used as an anode for lithium-ion batteries (LIBs), the FeP@NC@rGO anode demonstrates superior lithium storage properties, delivering a high specific capacity of 830 mA h g^{-1} after 100 cycles at 100 mA g^{-1} and an excellent rate capability of 359 mA h g^{-1} at 5 A g^{-1}. The outstanding performance is mainly due to the synergistic effect of the double carbon coating and the porous structure design. The introduction of porous carbon and graphene coating on FeP nanoparticles greatly enhances the electronic conductivity of the active material and well accommodates the large volume variation of FeP during the cycling process. Zhu *et al.* successfully developed a novel octahedral multi-channel FeP@C/rGO composite has been fabricated by a simple solvothermal process followed by carbonization and phosphorization.[81] Consequently, the as-prepared FeP@C/rGO electrode exhibits high reversible specific capacity (1080 mA h g^{-1} at the 0.1 A g^{-1}), superior cycling stability with a low-capacity decay rate (~0.04% per cycle upon 500 cycles at 1 A g^{-1}), and high specific capacity (497 mA h g^{-1}) even at a high current density of 5 A g^{-1}. The

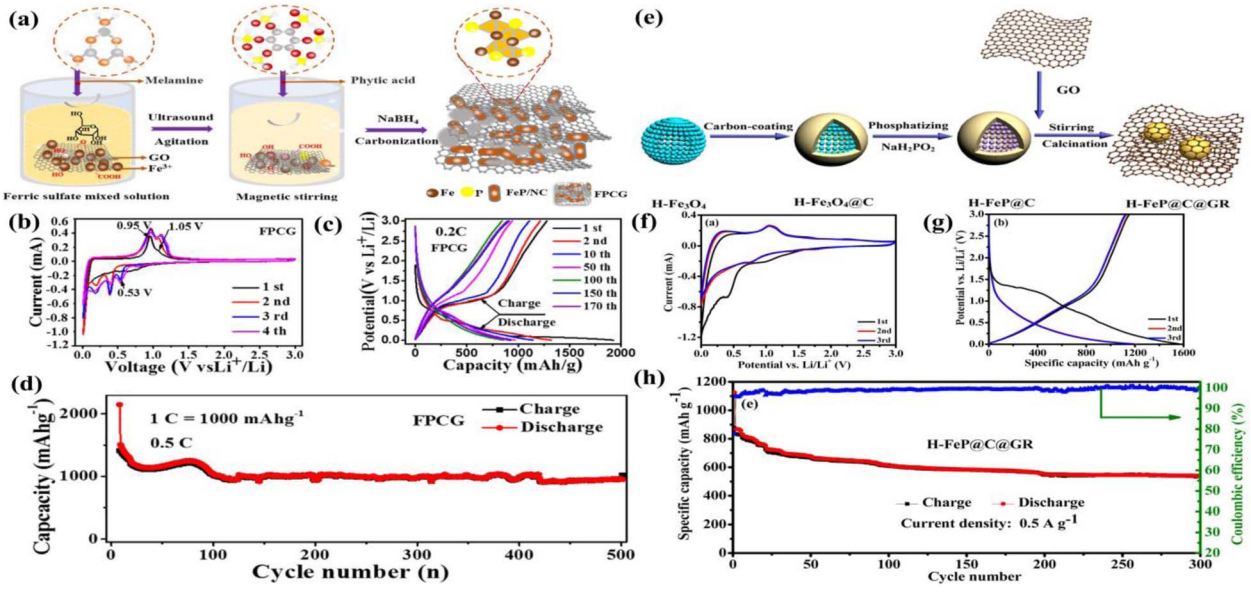

Fig. 6 (a) Schematic of the fabrication process of FPCG. (b) CV curve of FPCG nanocomposite at 0.1 mV s^{-1}. (c) The charge–discharge voltage distributions at 1, 2, 10, 50, 100, 150, and 170 cycles for FPCG electrodes in the voltage range of 0.01–3.0 V (*vs.* Liþ/Li) at 0.2C. (d) Long cycling performance of FPCG composite at a current density of 0.5C. (e) The detailed preparation procedure of 3D H-FeP@C@GR. (f) CV at the scan rate of 0.1 mV s^{-1} in the 0–3.0 V voltage range. (g) The first three discharge–charge curves of H-FeP@C@GR nanocomposite anode at a current density of 0.2 A g^{-1} in a voltage window of 0.005–3 V. (h) The long-term cycling performance of the H-FeP@C@GR nanocomposite at a current density of 0.5 A g^{-1}.

outstanding performance is mainly due to the octahedral carbon framework, which provides a multi-channel structure to facilitate the transport of ions and electrons. Furthermore, the FeP@C octahedra composites were stably interconnected with rGO nanosheets to construct a 3D structure, which mitigates pulverization and enhances conductivity. And, N/P co-doping improves the electrical conductivity of the FeP@C/rGO composite.

Liu *et al.* successfully developed a new FeP anode based on the electrochemical mechanism, and we propose a graphene oxide (GO) modification strategy to design and fabricate a FeP@GO anode with high electronic conductivity and structural stability.[82] The utilization of FeP@GO as an anode material for lithium-ion batteries demonstrated an average specific capacity of approximately 829.7 mA h g^{-1} for LIBs across the 2nd to 100th cycles, representing a 99% enhancement in comparison to the pure FeP (417.0 mA h g^{-1}). Jiang *et al.* achieved the successful synthesis of strongly coupled FeP@reduced graphene oxide (FeP@rGO) nanocomposites through the low-temperature phosphorization of aFeOOH@graphene oxide (a-FeOOH@GO).[83] The high mechanical strength and structural flexibility of graphene, which serve to buffer mechanical strain, and the high conductivity, which facilitates fast electron transport, have been demonstrated to be the key factors responsible for enhancing the lithium storage performance of FeP@rGO nanocomposites. Consequently, the as-prepared FeP@rGO nanocomposites exhibit excellent electrochemical performance. The electrochemical performance of the nanocomposites was found to be optimal for those prepared with a mass ratio of 1 : 5 (graphene oxide to $FeCl_3 \cdot 6H_2O$). The reversible discharge capacity of this nanocomposite is as high as 1000 mA h g^{-1} at 100 mA g^{-1} after 100 cycles. Furthermore, an ultra-stable capacity of 460 mA h g^{-1} could be achieved and maintained for 400 cycles at a high current density of 1000 mA g^{-1}. Luo *et al.* successfully developed a novel three-dimensional graphene framework, comprising FeP nanoparticles, which was designed and fabricated *via* a three-step method.[84] The hierarchical graphene framework has been demonstrated to enhance the electron conductivity of 3D FeP-rGO composites. Of particular significance is the 3D porous structure, which provides plentiful channels to facilitate rapid Li^+ diffusion and accommodate volume changes in FeP. This prevents capacity loss and ensures stable cycling performance of the 3D FeP-rGO anode for advanced LIBs. Therefore, the 3D FeP-rGO anode displays a considerable reversible cycling capacity (876 mA h g^{-1} at 0.5 A g^{-1} after 200 cycles), a robust long cycling capacity (448 mA h g^{-1} after 500 cycles at 3 A g^{-1}), and an impressive high-rate capacity (458 mA h g^{-1} at 10 A g^{-1}). Moreover, the full cell comprising a $LiFePO_4$ cathode exhibits a high reversible capacity of 373 mA h g^{-1} at 0.5 A g^{-1} following 120 cycles. Huang *et al.* developed a new FeP@C/reduced graphene oxide (rGO) anode material with a distinctive polyhedral structure. This was achieved through a straightforward solvothermal process and low-temperature phosphiding method.[85] The optimized FeP@C/rGO anode material demonstrated a discharge capacity of 414.7 mA h g^{-1} at a current density of 8 A g^{-1} and reached a capacity of 949.7 mA h g^{-1} after 100 cycles at 0.1 A g^{-1}. Even when cycled at a current density of 1 A g^{-1}, it provided a capacity of 737.7 mA h g^{-1} after 450 cycles. The FeP@C/rGO sample displayed improved stability and conductivity, due to two main factors. The MOF material's large surface area provides active sites and functions as a sacrificial template for the formed carbon skeleton, effectively mitigating volume change. *In situ* rGO coating forms a 3D network, accelerating electron and ion migration while suppressing nanoparticle aggregation.

Wang *et al.* present a rational design of graphene (GR) encapsulated with a hollow FeP@carbon nanocomposite (H-FeP@C@GR) *via* a combination of the following processes: hydrothermal route, carbon coating process, phosphidation treatment, and carbothermic reaction (Fig. 6e).[86] When H-FeP@C@GR nanocomposite was used as an anode material for LIBs at different current densities in Fig. 6g shows the charge/discharge processes (0.2, 0.5, 1, 2, 4, and 8 A g^{-1}), the capacity can still be recovered to 953 mA h g^{-1}. This material displays exceptional electrochemical performance as illustrated in Fig. 6f–h. The essential functions of GR in the transformation of a basic FeP@carbon nanocomposite into a sophisticated 3D network nanocomposite are as follows: (1) the 3D Omni-bearing conductive networks derived from the GR skeleton and outer carbon coating facilitate rapid diffusion of electrons and ions, thereby accelerating the electrode reaction kinetics. (2) The GR, which forms a cage-like framework around the H-FeP@C nanospheres, plays a crucial role in preventing the agglomeration of active materials and the cracking of the electrode. (3) The substantial volume alteration of H-FeP@C during the Li^+ insertion–extraction process can be mitigated through accommodation by the elastic GR, along with the available internal voids, thus ensuring the structural integrity of the electrode.

2.3 FeP with heterogeneous structure

The combining of FeP with other compounds to construct heterojunction composites with multi-structural/component advantages can enhance lithium-ion reaction kinetics, accelerate interfacial charge separation and electron conduction, improve lithium storage capacity, and reduce lithium storage stress. Yao *et al.* employed a one-pot approach to facilitate the formation of spherical FeNi-MOFs. Following annealing and phosphatization, FeP/Ni_2P/C@C nanoparticles were encased in a carbon shell derived from PVP, resulting in a yolk-shelled structure with voids (Fig. 7a).[87] As a lithium-ion anode material, the reversible capacity of FeP/Ni_2P/C@C nanospheres was 426 mA h g^{-1} at a current density of 0.5 A g^{-1} after 100 cycles. Even at the elevated current density of 1 A g^{-1}, the capacity was still retained at 364 mA h g^{-1}. As illustrated in Fig. 7b and c, the presence of other excellent electrochemical properties is also demonstrated. The distinctive yolk-shelled structure and synergistic effect of carbon in the FeP/Ni_2P/C@C electrode may be the cause of its excellent electrochemical performance (Fig. 7d). The structure enables volume expansion, increases electrical conductivity, and accelerates the diffusion of Li^+ ions and electrons during the charge/discharge process. Zheng *et al.* employed free-standing Fe_2O_3@FeP nanorod arrays anchored

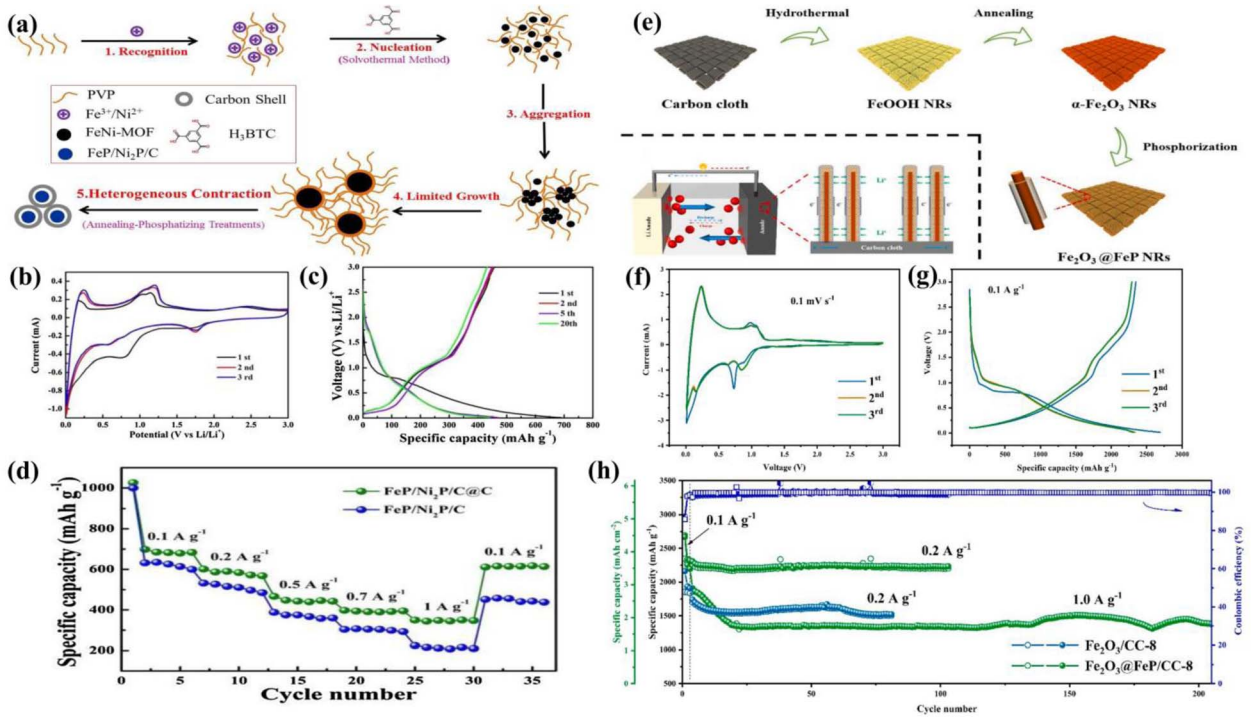

Fig. 7 (a) Possible formation mechanism of FeP/Ni_2P/C@C microspheres. (b) CV curves for the first three cycles of FeP/Ni_2P/C@C in the potential region of 0.01–3 V at a scan rate of 0.1 mV s^{-1}. (c) Charging–discharging curves for the 1st, 2nd, 5th, and 20th cycles of FeP/Ni_2P/C@C at 0.5 A g^{-1}. (d) Rate capability of FeP/Ni_2P/C@C and FeP/Ni_2P/C at different current densities. (e) Synthetic procedure illustration of the Fe_2O_3@FeP nanorods on CC. (f) CV curves at 0.1 mV s^{-1} of the Fe_2O_3@FeP/CC-8 electrode. (g) The initial three galvanostatic charge–discharge curves of the Fe_2O_3@FeP/CC-8 electrode at 0.1 A g^{-1}. (h) Long-term cyclic performance at 0.2 A g^{-1} and 1.0 A g^{-1}, respectively. The initial three charge–discharge profiles are at 0.1 A g^{-1}.

on carbon cloth (denoted as Fe_2O_3@FeP/CC) through a combined hydrothermal method and gas-phase phosphorization treatment (Fig. 7e).[88] When employed as an anode material, Fe_2O_3@FeP/CC-8 Fig. 7f and g displays superior reversible capacity (2692 mA h g^{-1} at 0.1 A g^{-1}), remarkable cycling stability (2232 mA h g^{-1} after 100 cycles at 0.2 A g^{-1}), and Fig. 7h shows the excellent rate capability (49% capacity retention from 0.1 to 2.0 A g^{-1}). The favorable electrochemical characteristics are ascribed to the FeP in conjunction with the CC substrate, which is capable of establishing bi-continuous conductive networks to facilitate electron transfer and enhance structural resilience. Furthermore, the open porous arrays and FeP with a considerable bonding distance can facilitate electrolyte impregnation and Li^+ migration, thereby effectively enhancing the rate capability. Li *et al.* have successfully synthesized a nanocube-like composite comprising heterostructured Fe_3O_4/FeP@C through a straightforward hydrothermal and post-heat treatment phosphating process.[89] As a consequence, the Fe_3O_4/FeP@C electrode exhibits an ultrahigh specific capacity and remarkable cyclic stability, sustaining robust cyclic stability with a capacity of 379.4 mA h g^{-1} after 800 cycles even at a high current density of 2000 mA g^{-1}. The Fe_3O_4/FeP@C electrode displays superior multiplication capability, competitive capacity, and satisfactory cycle life, which can be attributed to the enriched heterointerfaces within Fe_3O_4/FeP@C. These promote the generation of the built-in electric field, providing abundant electrochemical active sites that accelerate charge and ion diffusion, leading to excellent reaction kinetics. The core–shell nanostructure, in conjunction with a thin carbon-coated layer, serves to effectively mitigate structural strain and accommodate volume fluctuations during the cyclic process. This also facilitates comprehensive infiltration of each Fe_3O_4/FeP@C nanoparticle with electrolyte, thereby ensuring sufficient reaction and a prolonged cyclic lifespan. Furthermore, the assembly of numerous nanocubes results in the formation of a distinctive hierarchical structure, which establishes a robust, interconnected, and conductive network for rapid ion and electron transfer. Furthermore, the hierarchical structure prevents aggregation of the Fe_3O_4/FeP nanoparticles, thereby ensuring the overall structural integrity of the electrode materials.

3 FeP anodes for sodium-ion batteries

FeP is a very promising embedding-conversion anode material, with low embedding voltage and a high theoretical specific capacity of 926 mA h g^{-1}. However, FeP mainly has poor conductivity and drastic volume changes in the intercalation-detachment process, resulting in poor rate performance and cycling performance. Therefore, it has been used in FeP composites by better modification methods to prepare anode materials for sodium-ion batteries with excellent performance.

Sedation was confirmed as an insertion/conversion type reaction as follows:

$$FeP + xNa^+ + xe^- \leftrightarrow Na_xFeP$$

$$Na_xFeP + (3 - x)Na^+ + (3 - x)e^- \leftrightarrow Na_3P + Fe$$

3.1 FeP with structural regulation

Jiang *et al.* demonstrate the successful construction of a sodium-ion full cell by coupling a tubular PB cathode (T-PB) with its derived FeP anode (T-FeP) (Fig. 8j).[90] The tubular configuration endows the PB with rapid reaction kinetics, thereby enabling a high specific capacity of 94.4 mA h g^{-1} even at a high rate of 5.0 A g^{-1}. It is noteworthy that the assembled sodium-ion full cell demonstrates an unparalleled capacity of 105.3 mA h g^{-1} at 2.0 A g^{-1} and exhibits a robust cycling lifespan. As demonstrated in Fig. 8k–m, the other electrochemical properties are also of a high caliber. The favorable electrochemical properties of the T-PB cathode are attributed to its tubular structure, which facilitates the enlargement of the electrode/electrolyte contact areas and the implementation of a fast surface intercalation-controlled Na-storage mechanism. Furthermore, the tube framework confines the FeP nanoparticles (~10 nm) into the conductive carbon matrix, which enhances the reaction kinetics. Wang *et al.* have successfully synthesized binder-and-additive-free FeP nanorods grown on a titanium plate (FeP NRs/Ti) to enhance its sodium-ion diffusion capability.[91] The FeP NRs/Ti electrode demonstrated an exceptional rate capability, with specific capacities of 414.7, 372.4, 300, 252.6, and 196.2 mA h g^{-1} at current densities of 100, 200, 500, 1000, and 2000 mA g^{-1}, respectively, all based on the mass of FeP. Murali *et al.* present a straightforward, vapor-phase conversion of prominent metal oxalates into metal phosphide nanostructures (FeP), with a particular focus on their potential application in sodium-ion batteries (Fig. 8a).[47] Furthermore, this metal phosphide has been employed in sodium-ion batteries, where the capacity of the FeP anode at NIB was 216 mA h g^{-1} at a specific current of 100 mA g^{-1}, even after 100 cycles (Fig. 8i). As illustrated in Fig. 8g and h, the presence of other excellent electrochemical properties is also demonstrated. In general, FeP electrodes function as anodes for alkali ions with greater capacity, rate capability, higher coulombic efficiency, more stable cycling, and superior kinetics. In general, FeP electrodes function as anodes for alkali ions with greater capacity, rate capability, higher coulombic efficiency, more stable cycling, and superior kinetics.

3.2 FeP with carbon composite

Lim *et al.* synthesized the material through the low-temperature phosphorization of a metal–organic framework (MOF) nanostructure, resulting in a FeP/C composite with a highly porous nanocubic structure. This structure, characterized by FeP nanoparticles dispersed throughout the carbon scaffolding, exhibits a high surface area and a small pore size distribution, which offer potential applications in various fields.[92] Due to the distinctive porous structure of the FeP/C nanocubes, they display exceptional sodium storage characteristics. These include high capacity (410 milliampere hours per gram, 100 milliamperes per gram), excellent rate capacity (up to 1 milliampere per gram), and a lengthy cycle life exceeding 200 cycles. The enhanced performance of the SIBs and HER of FeP/NC can be attributed to three factors: the uniform morphology, the larger surface area, and the conductive carbonaceous framework, which collectively enhance the capacity and stability at all

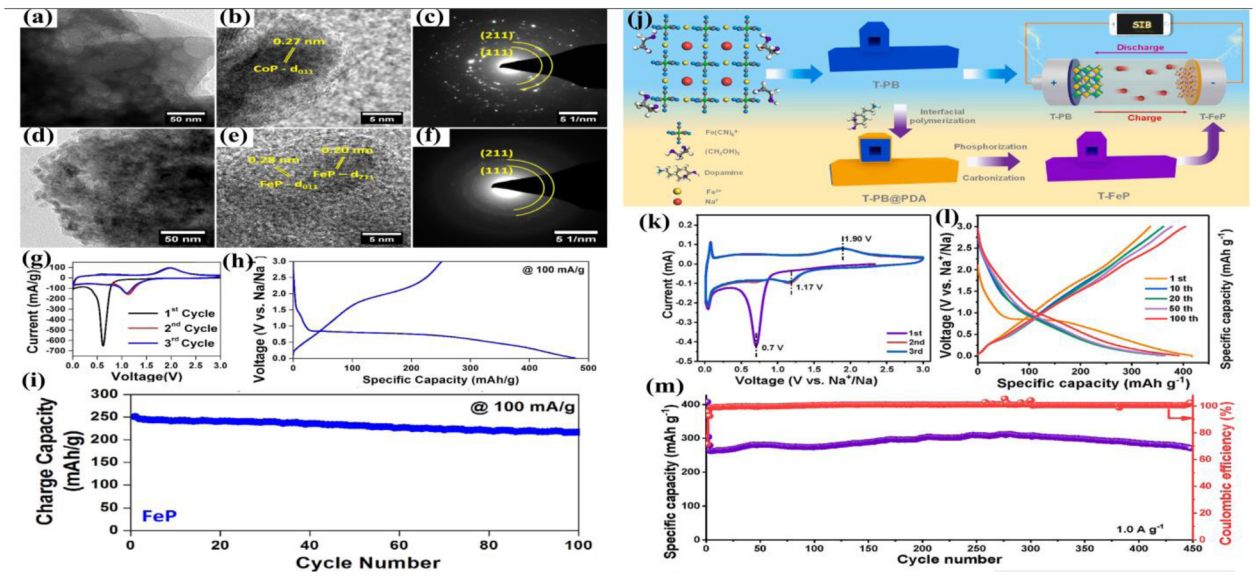

Fig. 8 (a–f) Possible formation mechanism of FeP/Ni_2P/C@C microspheres. (g) Cyclic voltammetry of FeP at a scan rate of 0.1 mV s^{-1}. (h) The adjacent first charge–discharge profiles of FeP for NIB. (i) Electrochemical cycling data for FeP at 100 mA g^{-1}. (j) Schematic diagram for the synthesis of T-PB and T-FeP. (k) CV curves at 0.2 mV s^{-1}. (l) Galvanostatic charge/discharge curves at 0.1 A g^{-1}. (m) Long-term cycling stability at 1.0 A g^{-1}.

rates of cycling. Wu *et al.* have developed a simple electrodeposition technique for the fabrication of hierarchical iron phosphide structures on biomass carbon membranes. The objective of this approach is to enhance the cyclability of iron phosphide-based anode materials for sodium-ion batteries (Fig. 9a).[93] The distinctive structure of the iron phosphides nanosheets/biomass carbon membrane enables the electrodes to demonstrate a specific capacity of 500.9 mA h g^{-1} at a current density of 50 mA g^{-1} after 100 cycles. Even when subjected to a high current density of 500 mA g^{-1}, the electrodes demonstrated remarkable stability, retaining 197 mA h g^{-1} after a prolonged testing period of 500 cycles (Fig. 9d). Fig. 9b and c shows the favorable electrochemical properties are ascribed to the nanosheets structure, which is advantageous for augmenting the specific surface area to facilitate the access of sodium ions and reduce the ion diffusion path. Concurrently, the interconnected porous structure in the biomass carbon membrane not only constrains the iron phosphide but also enhances the conductivity of the entire electrode for expeditious electrochemical reactions. Ren *et al.* have successfully synthesized two-dimensional (2D) nanosheet-like FeP/C composites from a precursor of a metal-oleate complex, employing a salt-template method (Fig. 9e).[94] In particular, the thin and uniform SEI layer formed on the FeP/C electrode surface could serve to further stabilize the interface and facilitate the rapid transfer of Na^+, thus enabling a capacity increase from 363.5 to 516.6 mA h g^{-1} at 0.1 A g^{-1} and superior rate/cycling properties (Fig. 9f). As shown in Fig. 9g–h, it has good electrochemical properties.

Initiated in the previous section, the discussion about carbon coating of FeP anode materials, we now proceed to the topic of integrating these carbon-coated materials with carbon nanomaterials. This combination is expected to bring into play the synergistic effects between carbon coating and carbon nanomaterials for improved electrochemical performance. In a recent publication, Wang *et al.* present a novel one-dimensional hierarchical material, consisting of carbon-coated mini hollow FeP nanoparticles homogeneously encapsulated in porous carbon nanofibers (denoted as M-FeP@C) through a low-temperature phosphidation method.[61] The M-FeP@C hybrid nanofibres demonstrate a high specific capacity and long cycling stability, exhibiting a capacity of 474 mA h g^{-1} after 100 cycles at 0.1 A g^{-1} as an anode for sodium-ion batteries. The remarkable electrochemical performance of the M-FeP@C hybrid nanofibres for sodium storage can be ascribed to the advantageous embedding architecture between the mini hollow FeP nanoparticles and double carbon layers scaffold. This configuration offers a continuous conducting framework and nanoporous channels for efficient ion and electron diffusion and transport, while also providing sufficient void space to accommodate volume changes during cycling. Yang *et al.* have successfully demonstrated that a high-capacity anode for SIBs can be developed by confining FeP nanoparticles in porous and electrically conductive carbon nanofibres (NFs) through a combination of electrospinning, carbonization, oxidation, and phosphidation procedures.[62] It is noteworthy that the composite exhibit offers structural advantages over FeP without a carbon matrix. This is because the FeP nanoparticles embedded in a carbon matrix become more structurally stable and have faster pathways for electron and ion transport. These features have enabled a high capacity in LIBs (~1160 mA h g^{-1}) and SIBs (760 mA h g^{-1}), along with excellent stability over 300 low-rate cycles and 1000 high-rate cycles. Gao *et al.* developed a generalized strategy for the synthesis of unique bowl-like hollow particles consisting of dual-carbon-protected ultrasmall iron-based compound nanodots

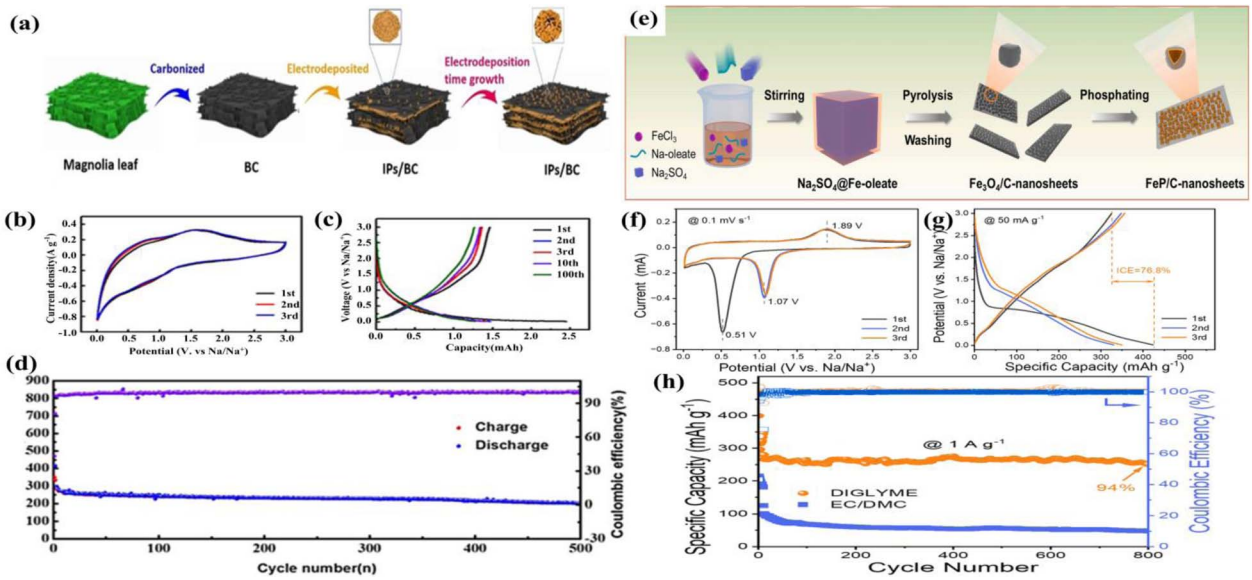

Fig. 9 (a) Schematic illustration of the synthesis of the IPs/BC composite. (b) CV curves at a scan rate of 0.1 mV s^{-1}. (c) Discharge–charge curves at 50 mA g^{-1}. (d) Cycling performances of the IPs/BC electrodes at 500 mA g^{-1}. (e) Schematic synthesis diagram of the FeP/C nanosheets. (f) CV curves at 0.1 mV s^{-1}. (g) Charge/discharge profiles in DIGLYME electrolyte at 50 mA g^{-1}. (h) Comparison of cycling performance at 1.0 A g^{-1} in DIGLYME and EC/DMC electrolytes.

embedded into a carbon matrix (denoted as C@FeP).[95] The C@FeP demonstrated remarkable cycling stability, retaining a high energy density of 85.1 W h kg^{-1} under a high rate of 1.0 A g^{-1} and exhibiting an impressive retention percentage of 84.6% after 1000 cycles. Notably, the iron-based bowl-like hollow particles demonstrated an exceptional capacity for sodium storage, displaying a high specific capacity, excellent cycling stability, and rate capabilities. Ma *et al.* demonstrate an anode composed of carbon-coated FeP nanoparticles anchored to carbon nanotube networks (CNT@FeP-C), which effectively retain the FeP nanoparticles within flexible carbon hosts while simultaneously maintaining monodispersity among these hosts.[96] When evaluated as the anode for sodium-ion batteries (SIBs), the CNT@FeP-C composite electrode demonstrated exceptional cycling performance and superior rate capability. This unique structure exhibited remarkable long-term cycling stability, retaining 95% of its capacity after more than 1200 cycles at a current density of 3 A g^{-1}, and achieving a rate capability of 272 mA h g^{-1} at 8 A g^{-1}. The excellent electrochemical properties can be attributed to the interconnected conductive network formed by carbon nanotubes (CNTs) and the carbon shell surrounding the nanoparticles. This network facilitates rapid electron and ion transfer and transport, thereby promoting superior rate capability. Shi *et al.* report the self-confined growth of FeP quantum dots on a CNT-grafted, phosphorus-doped 3D octahedral carbon framework (FeP@OCF/CNT) achieved through an *in situ* reductive phosphatization and carbonization of a metal–organic framework (Fig. 10a).[97] When evaluated as the anode for sodium-ion batteries (SIBs), the material demonstrates an exceptional reversible capacity of 674 mA h g^{-1} at a current density of 0.1 A g^{-1}, alongside a record high-rate performance of 262 mA h g^{-1} at 20 A g^{-1}. This synthesis involves the direct growth of FeOOH on the CNTs, followed by silica coating, carbon coating, and subsequent low-temperature phosphidation and silica removal treatments. As shown in Fig. 10b–d, it has good electrochemical properties. This unique architectural design offers several advantages for high-rate and stable sodium storage: (i) the 3D P-doped carbon octahedra, grafted with 1D CNTs, serve as an electrical highway for rapid electron transport; (ii) the carbon framework restricts the growth of FeP quantum dots to less than 10 nm, thereby reducing the charge transfer length within the TMP particle; (iii) the 3D carbon octahedral framework, characterized by its highly porous structure, functions as a sodium ion reservoir, facilitating the diffusion of Na^+ ions while simultaneously buffering volume changes and preventing the aggregation of FeP nanoparticles during cycling. Han *et al.* developed a synthetic strategy based on the concept of nanoconfinement reactions to construct carbon-coated iron phosphide (FeP) with an amorphous and mesoporous framework anchored on carbon nanotubes (CNTs) (Fig. 10e).[98] When utilized as an anode material in sodium-ion batteries (SIBs), the FeP-based electrode demonstrates an active material utilization rate of 78% and a reversible capacity of 415 mA h g^{-1}. Even at an elevated current density of 500 mA g^{-1}, the electrode retains 90% of its capacity over 500 cycles, exhibiting a minimal capacity decay rate of only 0.02% per cycle (Fig. 10h). This can be observed when the designed nanocomposite is applied as anodes in sodium-ion batteries (SIBs), where it demonstrates significantly improved performance in Fig. 10f and g shows the terms of specific capacity and cycle life.

3.2.1 FeP with heteroatom doping. Li *et al.* have successfully synthesized N-doped carbon layer-coated yolk-shelled Cu-

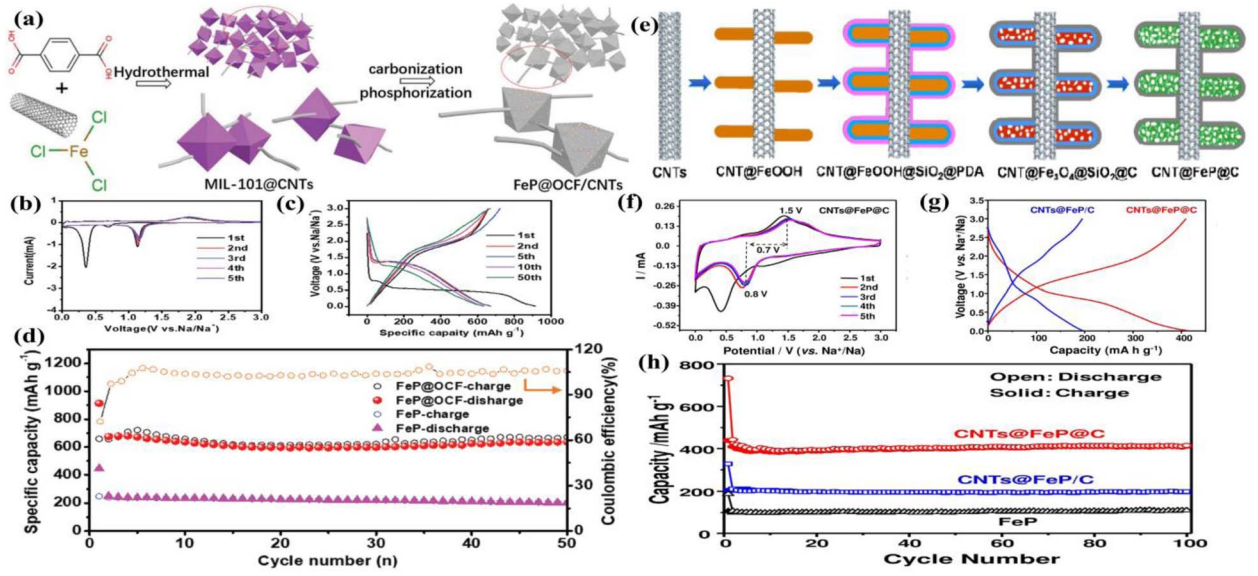

Fig. 10 (a) Schematic diagram for the synthesis of FeP@OCF. (b) CV curves of FeP@OCF between 0.01 and 3 V *versus* Na/Na^+. (c) Charge–discharge profiles of FeP@OCF electrode at 0.1 A g^{-1}. (d) Cycling performance of the FeP@OCF and FeP electrode at the current density of 0.1 A g^{-1}. (e) Schematic illustration of the principal steps in the preparation of carbon-coated CNT@FeP with an amorphous and mesoporous structure. (f) Cyclic voltammograms of CNT@FeP/C at 0.1 mV s^{-1}. (g) Charge–discharge voltage profiles of the 100th cycle. (h) The cycle performance of CNT@FeP@C, CNT@FeP/C, and FeP at a current density of 100 mA g^{-1}.

doped FeP (denoted as YS-Cu-FeP@C) spheres *via* a templating strategy (Fig. 11a).[99] The synthesis of YS-Cu-FeP@C spheres affords a unique compositional and structural advantage, which in turn leads to enhanced electrochemical performance for SIBs. This includes excellent rate capability (145 mA h g^{-1} at 10 A g^{-1}) and Fig. 11d shows the remarkable long-term cycle performance (up to 900 cycles at 1 A g^{-1}). The enhanced electrochemical performance of YS-Cu-FeP@C spheres for sodium storage is attributable to their distinctive structure and composition. As shown in Fig. 11b and c, it has good electrochemical properties. The yolkshelled structure facilitates the rate of reaction between Na^+ and the electrode, and can effectively buffer the volume expansion that occurs during the charging and discharging processes. The N-doped carbon can enhance the conductivity and promote structural stability upon sedation/dissociation. C doping can enhance the electronic conductivity of FeP and facilitate the migration of Na^+. Li *et al.* have an open-framework structure in which ultrafine FeP nanodots are fully embedded in 3D mesoporous nitrogen-doped carbon nanosheets (FeP@NC).[100] The prepared FeP@NC has been shown to exhibit excellent rate capability and remarkable long-term cycling performance when used as an SIB anode. A stable reversible capacity of 374 mA h g^{-1} can be obtained at 0.5 A g^{-1} for 2000 cycles with a markedly low capacity decay of 0.01% per cycle. Even at a high current density of 5 A g^{-1}, a specific capacity of 201 mA h g^{-1} can be achieved. The favorable electrochemical properties of the material are ascribed to the uniform distribution of ultrafine FeP nanodots within the nitrogen-doped carbon nanosheets (NC), which are connected to form an open-framework structure, FeP@NC, comprising abundant interconnected mesopores and a high specific surface area. The meticulously designed structure not only guarantees the structural integrity of FeP@NC during repeated cycles but also ensures rapid electrode reaction kinetics. Wang *et al.* synthesized a coral-like FeP composite with FeP nanoparticles anchored and dispersed on a nitrogen-doped three-dimensional carbon framework (FeP@NC) through an *in situ* phosphating/carbonization process of polymer precursors (6h-FeP@NC-1).[71] The FeP@NC composite exhibits a reversible capacity of 90.4 mA h g^{-1} after 10 000 cycles at 10 A g^{-1}, with a capacity retention of 82.0% for SIBs, which represents a significant improvement over previously reported FeP-based composite. Furthermore, the composite exhibited a capacity retention of 90.3% for LIBs, with a specific capacity of 179.4 mA h g^{-1} after 5000 cycles at 10 A g^{-1}, which has surpassed the majority of previously reported FeP-based composites. The findings demonstrated that the refinement of FeP nanoparticles could promote the formation of a greater quantity of graphitized carbon, as a consequence of improved absorption capabilities throughout cycling. This increased graphitization provides additional locations for the intercalation of Na^+ ions, thereby enhancing storage capacity. Concurrently, an increment in interfacial magnetization, resulting from the refinement of FeP nanoparticles, contributes to the development of supplementary capacitance. Saleem *et al.* have successfully synthesized N, P-codoped onion-like carbon (NPOLC)-encapsulated FeP (FeP@NP-OLC) using a simple injection pyrolysis method, followed by a successive low-temperature phosphidation treatment (Fig. 11e).[101] The FeP@NP-OLC-5 composite anode demonstrates a high reversible capacity of 543 mA h g^{-1} at 0.5 A g^{-1} through 500 cycles and a specific capacity of 560 mA h g^{-1} at 1 A g^{-1} after 1100 cycles (Fig. 11h), for a sodium-ion battery. As shown in Fig. 11f and g, it has good electrochemical properties. The enhanced rate capability and sustained cycling performance can be attributed to the fact that the FeP@NP-OLC nanospheres not only enhance

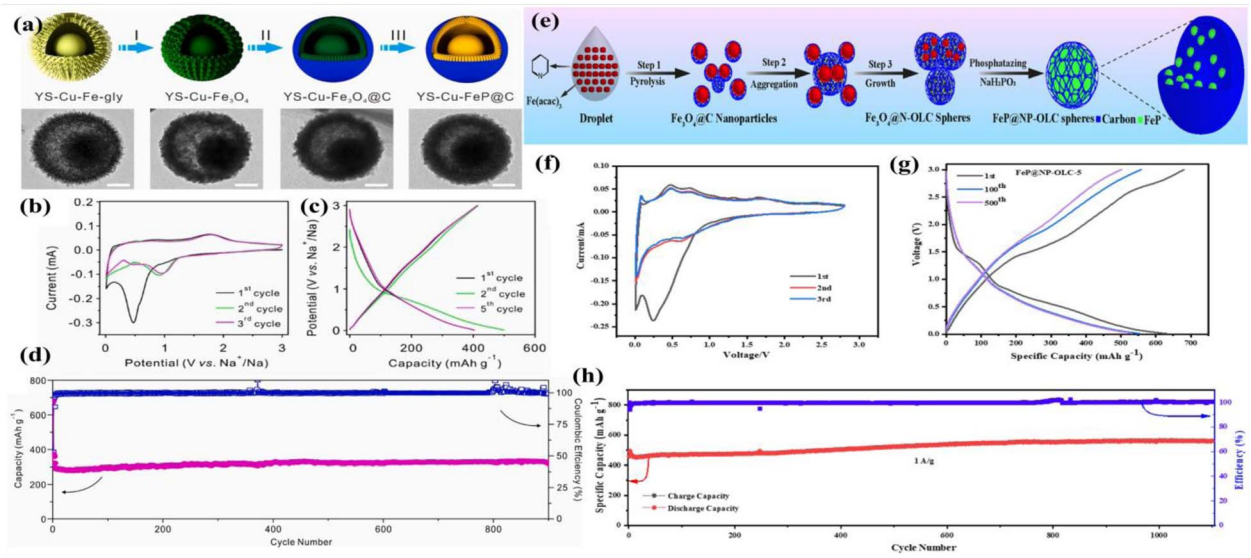

Fig. 11 (a) Schematic illustration of the formation of YS-Cu-FeP@C spheres. (b) The first to fifth cyclic voltammograms of the YS-Cu-FeP@C spheres electrode in 0.01–3.0 V. (c) Galvanostatic charge/discharge curves of the 1st, 2nd, and 5th cycles for the YS-Cu-FeP@C spheres electrode at 0.1 A g^{-1}. (d) Cycling stability of the YS-Cu-FeP@C spheres electrode at 1 A g^{-1}. (e) Schematic representation of the synthesis of an onion-like FeP/NP-OLC nanosphere. (f) CV curves of FeP/NP-OLC-5 at 0.1 mV s^{-1}. (g) Discharge and charge curve of FeP/NP-OLC-5 at 0.5 A g^{-1}. (h) Long cyclic performance of FeP/NP-OLC-5 at 1 A g^{-1} for 1100 times.

structural stability but also effectively cushion the volume expansion of FeP that occurs during repetitive cycling. Shi *et al.* have successfully reported a new binder-free anode material, namely an electrospun free-standing FeP@NPC film comprising FeP nanoparticles wrapped in 3D interconnected N,P-codoped carbon fibers, which exhibits high performance in sodium ion storage.[102] The battery exhibits a high reversible capacity of 557 mA h g^{-1} and a remarkable cycling life of 1000 cycles. The distinctive structural configuration bestows a multitude of advantageous characteristics. During the synthesis, the growth of FeP nanoparticles is constrained by the PAN nanofiber, preventing agglomeration. The 3D interconnected carbon fiber network functions as an electron and ion transport pathway, accelerating the reaction kinetics while accommodating the volume expansion of FeP during sodiation and desodiation. Zhao *et al.* have successfully presented hierarchical TMP-carbon hybrid structures composed of carbon-coated TMP nanoparticles embedded in P and N dual-doped porous carbon nanosheets (denoted as TMP@C-PNCNS, including FeP@C-PNCNS, CoP@C-PNCNS, and Ni_2P@C-PNCNS) through a facile, extensible, one-pot strategy followed by carbonization treatment. The dual-carbon protected, P and N dual-doped and hierarchical structure of the TMP@C-PNCNS anodes results in an extraordinary sodium-ion storage performance.[103] The prepared FeP@C-PNCNS anode benefits from enhanced electrical conductivity, a shortened electron/ion transport distance, and a greater abundance of active sites. Consequently, it exhibits superior long-term cycling stability at a high current density of 5.0 A g^{-1}, with capacity retention reaching 70.8% over 4000 cycles. Park *et al.* have successfully designed a densely packed free-standing film consisting of carbon-coated FeP nanoparticles anchored on P-doped graphene (FeP@C@PG film) through solventless thermal decomposition and the roll-press method.[104] The FeP@C@PG film exhibits a stable reversible capacity of 536.6 mA h g^{-1} after 1000 cycles at a current density of 1 A g^{-1}, demonstrating good capacity retention. Additionally, it shows an excellent rate capability of 440.7 mA h g^{-1} at a current density of 5 A g^{-1}, along with remarkable oxidation stability at 80 °C in air. Jiang *et al.* successfully developed a facile and eco-friendly approach for the *in situ* embedding of FeP nanoparticles in a honeycomb-like carbon matrix with N and P codoping (FeP@PNC) using green phytic acid (PA) as precursors.[105] The FeP@PNC electrode, serving as the anode for sodium storage, demonstrated superior reversible capacity (340.1 mA h g^{-1} at 0.1 A g^{-1}), excellent rate capability (84.1 mA h g^{-1} at 3 A g^{-1}), and prolonged cycling life (224.5 mA h g^{-1} over 4500 cycles at 0.5 A g^{-1}). The unique architecture of FeP@PNC offers distinct advantages: (a) ultrafine FeP nanoparticles reduce fracture risk during sodiation/desodiation by mitigating isotropic stress, (b) the 3D porous carbon matrix accommodates volume expansion and enhances ion/electron diffusion, and (c) *in situ* embedding prevents active particle aggregation and provides extensive interface contact for Na ion storage. This optimized structure results in outstanding long-life cycling stability and rate capability.

3.2.2 FeP with rGO composite. Jiang *et al.* successfully fabricated a hybrid nanostructured SIBs anode comprising FeP nanoparticles anchored on rGO nanosheets *via* a facile but effective *in situ* low-temperature chemical solution deposition-assisted phosphorization method (Fig. 12a).[106] Electrochemical characterization indicated that the FeP@rGO composite nanostructured anode delivers an attractive reversible capacity of up to 366.6 mA h g^{-1}, with superior cycling stability (388.8 mA h g^{-1} after 250 cycles) and high coulombic efficiency (>99%) in Fig. 12d. As illustrated in Fig. 12b and c, the material displays favorable electrochemical properties. The interlaced rGO stacks around FeP particles not only facilitate the uniform distribution of FeP nanoparticles on the rGO, but also enhance ion diffusion and electrical conductivity. Furthermore, the presence of cracks and pores among the rGO stacks also serves to reduce the distance that sodium ions must diffuse, thereby enhancing the rated capacity. Furthermore, the robust chemical bonding and extensive void space ensure structural stability even when the battery is fully discharged. Wang *et al.* have synthesized the FeP@C/rGO nanocomposite through the implementation of a three-stage process, beginning with a hydrothermal procedure, followed by rGO modification, and concluding with phosphorization (Fig. 12e).[107] The FeP@C/rGO nanocomposite displays excellent rate capability and long cycle life when employed as the anode of SIBs. In particular, the FeP@C/rGO nanocomposite exhibits high specific capacities of 635.7 and 343.1 mA h g^{-1} at 20 and 2000 mA g^{-1}, respectively (Fig. 12f and g), and demonstrates stable cycling with 88.2% capacity retention after 1000 cycles (Fig. 12h). The superior performance can be attributed to the rationally designed hierarchical porous FeP@C/rGO, which exhibits a high capacitive contribution of 93.9% (at 2 mV s^{-1}) and a small volume expansion of only 54.9%. Li *et al.* successfully synthesised FeP/RGO hybrids with adjustable graphene concentrations using facile chemical precipitation and low-temperature phosphorization method.[108] The resulting FeP/RGO electrode exhibited excellent electrochemical performance, with a high reversible capacity of 547 mA h g^{-1} at a current density of 100 mA g^{-1} after 100 cycles. Even at a current density of 2.0 A g^{-1}, the specific capacity of the FeP/RGO hybrid sample can still be maintained at 421 mA h g^{-1}, demonstrating a good and fast Na^+ charging capability. Therefore, the FeP/RGO nanocomposite exhibits both high rate capacity and long cycling performance. Wang *et al.* synthesized a distinctive hybrid architecture featuring iron phosphide nanodots anchored to 3D phosphorus-doped graphitic nitrogen-rich graphene (FeP/NPG). This architecture was produced through the phosphidation of NH_2-rich reduced graphene oxide (rGO) that had been decorated with Fe_2O_3.[109] The distinctive features of the FeP/NPG system yield exceptional sodium storage performance. A high reversible capacity of 613 mA h g^{-1} is achieved at a current density of 50 mA g^{-1}. Additionally, remarkable rate capabilities of 422 mA h g^{-1} and 349 mA h g^{-1} are observed at 1 A g^{-1} and 3 A g^{-1}, respectively. Furthermore, a remarkably stable capacity of 378 mA h g^{-1} at a current density of 1 A g^{-1} is maintained over extensive cycling. When evaluated as an anode material for sodium-ion batteries (SIBs), this architecture exhibits exceptional sodium storage performance, characterized by a high reversible discharge capacity, superior rate capability, and outstanding stability over extended cycling.

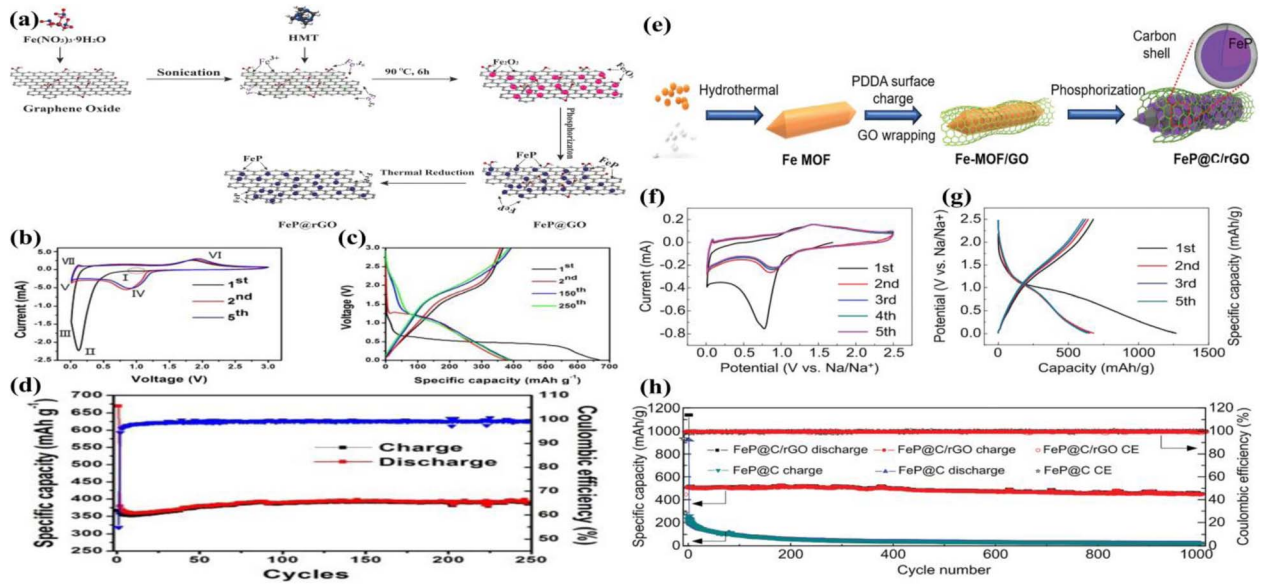

Fig. 12 (a) Schematic illustration of the preparation of FeP@rGO nanocomposite. (b) CV curves of FeP@rGO anode at the potential range from 0.01 to 3.0 V at a scan rate of 0.5 mV s^{-1}. (c) Typical charge–discharge curves of FeP@rGO anode at a current density of 0.1 A g^{-1} in a potential range of 0.01–3.0 V *vs.* Na/Na^+. (d) Cycling behavior of the FeP@rGO anode at a current density of 0.1 A g^{-1}. (e) Schematic diagram of the synthesis process of FeP@C/rGO nanocomposites. (f) CV curves of the FeP@C/rGO electrode of the first 5 cycles at a scan rate of 0.1 mV s^{-1} in the potential range of 0.01–2.5 V *vs.* Na/Na^+. (g) Galvanostatic discharge/charge curves of the FeP@C/rGO electrode of the first 5 cycles at a current density of 20 mA g^{-1}. (h) Long-term cycling performance and related coulombic efficiency of FeP@C/rGO and FeP@C nanocomposite electrodes at a current density of 200 mA g^{-1} for 1000 cycles.

3.3 FeP with heterogeneous structure

Park *et al.* have successfully prepared expanded sandwich-like porous heterostructures of swollen FeP NSs@rGO by a charge-driven self-assembly strategy and subsequent phosphating/annealing process.[110] When employed as anode materials for sodium-ion batteries, the expanded FeP NSs@rGO composite exhibits a high FeP content (52.3%) and noteworthy electrochemical performance. The expanded FeP NSs@rGO exhibits a high specific capacity of 916.1 mA h g^{-1} at 0.1 A g^{-1}, a superior rate capability of 440.9 mA h g^{-1} at 5 A g^{-1}, and a long-term cycling stability of 85.4% capacity retention after 1000 cycles at 1 A g^{-1}. Li *et al.* successfully synthesized unique core–shell porous FeP@CoP phosphide microcubes interconnected *via* reduced graphene oxide (RGO) nanosheets (RGO@CoP@FeP) for the first time using a low-temperature phosphorization process with Prussian blue as a reactant template.[111] The RGO@CoP@C-FeP electrode demonstrated impressive rate capability, exhibiting specific capacities of 480.2, 435.1, 403.3, and 374.6 mA h g^{-1} at current densities of 0.1, 0.2, 0.5, and 1 A g^{-1}, respectively. Furthermore, it maintained a capacity of 341.2 mA h g^{-1} at a high current density of 2 A g^{-1} and recovered to 468.3 mA h g^{-1} when the current density returned to 0.1 A g^{-1}, showcasing excellent electrochemical performance. Han *et al.* have successfully hetero-CoP/FeP nanoparticles embedded in porous carbon nanofibers (CoP/FeP@PCNFs) obtained by coaxial electrospinning and low-temperature phosphorization processes.[112] By employing CoP/FeP@PCNFs as the anode for sodium-ion batteries, a large reversible specific capacity (459 mA h g^{-1} at 0.05 A g^{-1}), excellent rate performance (46.4% capacity retention rate at 10 A g^{-1} relative to 0.05 A g^{-1}) and long-term cycling stability (208 mA h g^{-1} at 5 A g^{-1} over 1000 cycles and 73.5% capacity retention) can be obtained. Xiao *et al.* successfully constructed heterostructured Fe–Co–P (FeP/Co2P) arrays for sodium-ion batteries (SIBs) in this study (Fig. 13a).[113] The Fe–Co–P arrays demonstrated impressive performance, exhibiting high reversible capacities of 634 mA h g^{-1} at 0.2 A g^{-1} and 239 mA h g^{-1} after 300 cycles at 1 A g^{-1} (Fig. 13d). As illustrated in Fig. 13b and c, the material displays favorable electrochemical properties. These excellent electrochemical properties are attributed to the unique heterostructure, which contains abundant heterointerfaces that significantly mitigate volume changes during (de)sodiation and provide increased active sites for Na^+ ions. Mao *et al.* prepared bimetallic FeP/C@CoP composites using a two-step solvothermal method, exhibiting excellent reversible capacity when used as anodes for sodium-ion batteries.[114] The specific capacity of the FeP/C@CoP reached 275.7 mA h g^{-1} at a high current density of 5 A g^{-1} and remained as high as 321.9 mA h g^{-1} after 800 cycles at 1 A g^{-1}. Accordingly, the uniform embedding of FeP/CoP bimetal phosphide heterostructures into the carbon matrix led to a notable enhancement in both capacity and cycling stability. Ma *et al.* developed a three-dimensional (3D) FeP/CoP heterostructure embedded in N-doped carbon aerogel (FeP/CoP-NA) *via* an *in situ* process combining cross-linking and phosphorization (Fig. 13e).[115] This resulted in bimetallic FeP/CoP nanoparticles wrapped in N-doped carbon, forming a core–shell structure. Thanks to these favorable features, FeP/CoP-NA exhibited high rate performance (342 mA h g^{-1} at 5 A g^{-1}), enhanced specific capacity

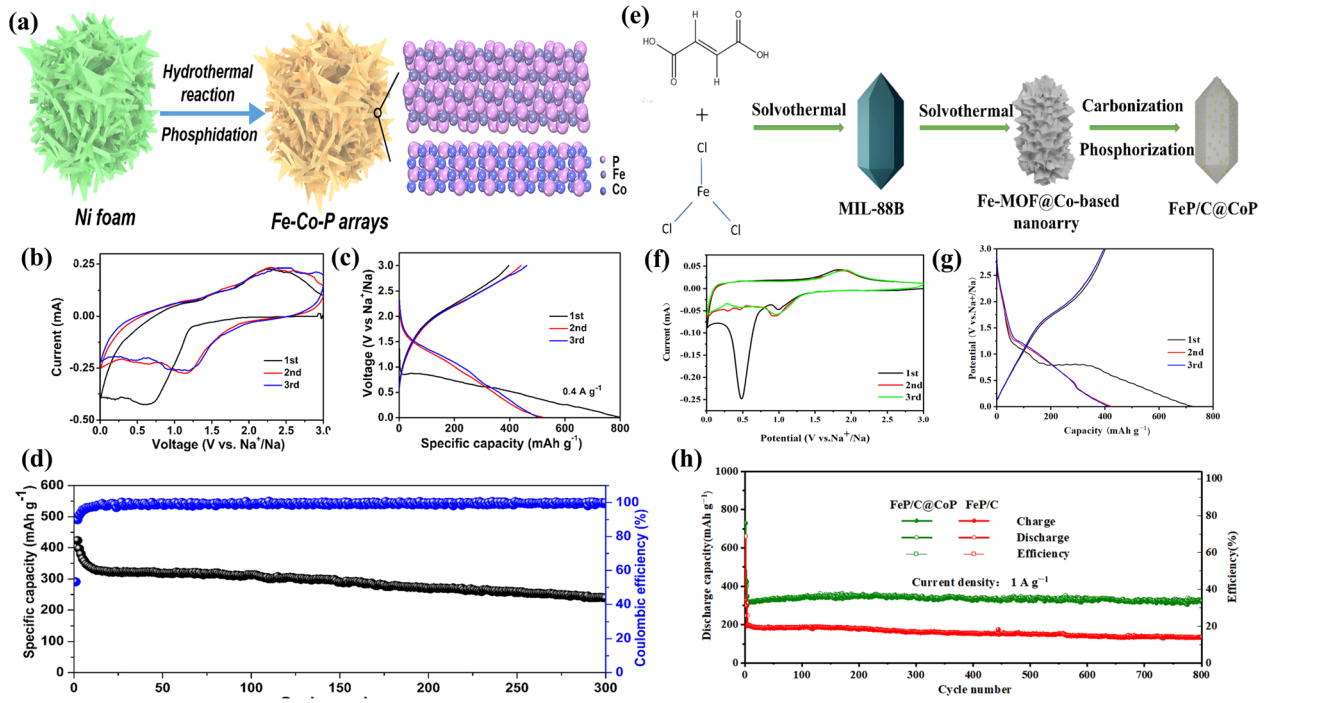

Fig. 13 (a) Schematic illustration of the preparation process of Fe–Co–P arrays. (b) CV curves of Fe–Co–P anode at 0.2 mV s^{-1}. (c) Charge–discharge curves of Fe–Co–P anode at 0.4 A g^{-1}. (d) Cycling performance at 1 A g^{-1} for the Fe–Co–P anode. (e) Schematic process of the synthesis process of the FeP/C@CoP composites. (f) The first three CV curves at 0.1 mv s^{-1} at 0.01–3.0 V. (g) The first three capacity–voltage curves at 0.1 A g^{-1}. (h) Long-cycle performance at 1 A g^{-1}.

(525 mA h g^{-1} at 0.2 A g^{-1}), and an ultralong cycling life (over 8000 cycles at 5 A g^{-1}) in Fig. 13f–h. Impressively, the successful construction of the atomic interface between FeP and CoP enhances capacitive contributions to facilitate electron transport and provides additional active sites for Na^+ adsorption. This unique interface is key to the material's excellent electrochemical performance.

4 FeP anodes for potassium-ion batteries

Phosphorus iron (FeP), as an anode material for potassium-ion batteries (PIBs), boasts several advantages such as high theoretical capacity, low cost, and strong electrochemical activity. However, it is hindered by its low electronic conductivity and significant volume strain. Furthermore, the reaction mechanism of FeP remains unclear and necessitates further investigation. Murali *et al.* present a straightforward, vapor-phase conversion of prominent metal oxalates into metal phosphide nanostructures (FeP), with a particular focus on their potential application in potassium-ion batteries.[47] When used as an anode material for potassium-ion batteries, FeP delivered a capacity of 195 mA h g^{-1} at a specific current of 100 mA g^{-1}. Overall, the FeP electrode exhibited excellent performance as an anode, demonstrating higher capacity, improved rate capability, enhanced coulombic efficiency, stable cycling, and better kinetics for alkali ions. Potassiumization was confirmed as an insertion/conversion type reaction as follows:

$$FeP + xK^+ + xe^- \leftrightarrow K_xFeP$$

$$K_xFeP + (3 - x)K^+ + (3 - x)e^- \leftrightarrow K_3P + Fe$$

$$K_xFeP \leftrightarrow FeP + xK^+ + xe^-$$

Yang *et al.* successfully synthesized uniform yolk–shell FeP@C nanoboxes (FeP@CNBs) with inner FeP nanoparticles fully protected by a thin, self-supported carbon shell through a phosphidation process using yolk–shell Fe_2O_3@CNBs as a precursor.[59] The rate capacity performance of both FeP@CNBs and FeP nanocubes was evaluated under various current densities ranging from 0.1 to 2 A g^{-1}. FeP@CNBs demonstrated reversible capacities of 201, 156, 101, 65, and 37 mA h g^{-1} at 0.1, 0.2, 0.5, 1, and 2 A g^{-1}, respectively. Additionally, the capacity of FeP@CNBs could be restored to 200 mA h g^{-1} when the current density returned to 0.1 A g^{-1}, highlighting its exceptional potassium storage performance. The unique structural features of FeP@CNBs contribute to their high reversible capacity, superior rate performance, and extremely stable cycling life.

Xu *et al.* successfully explored a simple method of *in situ* encapsulation of FeP nanoparticles in a porous carbon framework (FeP@C) through metal–organic framework (MOF)-derived phosphorization.[53] The FeP@C anode achieved a high reversible capacity of 163 mA h g^{-1} at 0.2 A g^{-1} over 100 cycles for K-ion batteries. This superior rate capability and ultra-stable cycling performance can be attributed to the 3D porous carbon-encapsulated FeP nanoparticles, which enhance structural

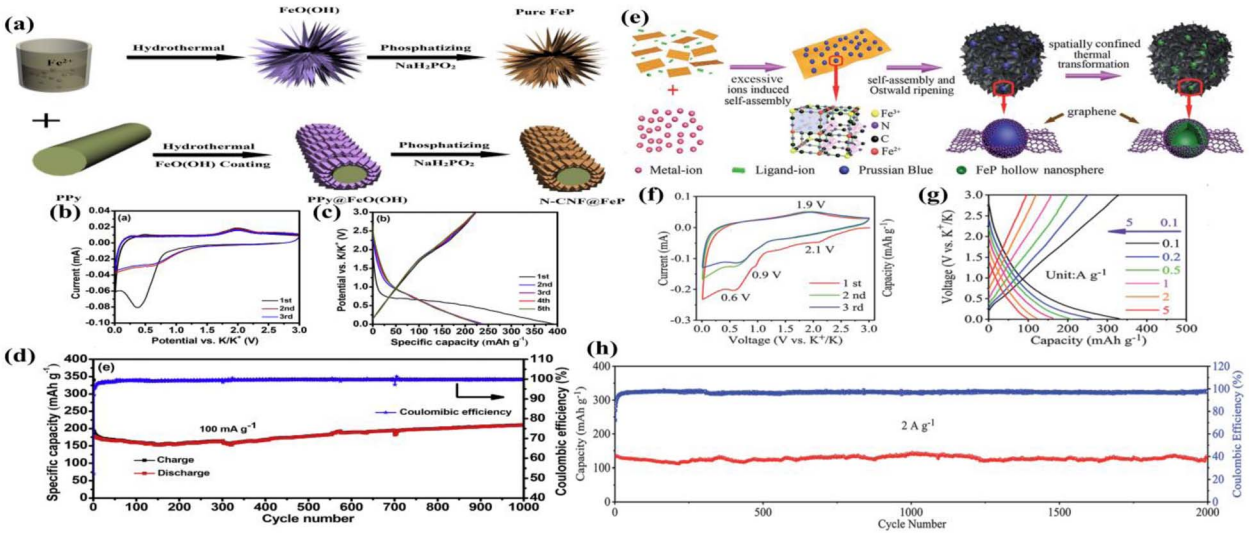

Fig. 14 (a) Schematic illustration of the synthesis process for NeCNF@FeP and pure FeP. (b) CV profiles of NeCNF@FeP electrode at a scan rate of 0.2 mV s^{-1}. (c) Discharge/charge profiles of NeCNF@FeP electrode. (d) Long-term cycling property and coulombic efficiency of NeCNF@FeP electrode at a current density of 100 mA g^{-1}. (e) Schematic illustration of the fabrication process of 3DG/FeP composite aerogel. (f) CV curves of 3DG/FeP at the scan rate of 0.2 mV s^{-1}. (g) Galvanostatic charge/discharge curves of 3DG/FeP at different current densities. (h) Cycling performance of 3DG/FeP at 2 A g^{-1} for 2000 cycles.

stability, enlarge active surface areas, improve electrical conductivity, promote ion/electron transport, and provide ample void space to alleviate volume expansion during repeated cycling. Tan *et al.* fabricated a three-dimensional (3D) foam-like graphene carbon scaffold incorporated with FeP nanoparticles (FeP@FGCS) using a straightforward pyrolysis-blowing and phosphorization approach.[116] As an anode material for potassium-ion batteries, FeP@FGCS demonstrated superior electrochemical activity for potassium storage, achieving a high capacity of 382 mA h g^{-1} at 0.1 A g^{-1} and exhibiting outstanding cycling performance, retaining 213 mA h g^{-1} over 800 cycles at 2 A g^{-1}. Therefore FeP@FGCS exhibits superior electrochemical activity for potassium storage, outstanding cycling performance, effective accommodation of volume expansion, and additional active sites for ion storage, making it an ideal electrode material for potassium-ion batteries. Li *et al.* successfully fabricated FeP and FeP/C composites using a facile and cost-effective high-energy ball-milling method.[117] The inclusion of carbon significantly improved the cycling and rate performance of the FeP/C composite. The FeP/C composite demonstrated a discharge capacity of 288.9 mA h g^{-1} at 50 mA g^{-1}, maintaining 112.52 mA h g^{-1} at a high current density of 500 mA g^{-1}, which is superior to pure FeP. Additionally, the composite retained a capacity of 178.56 mA h g^{-1} after 50 cycles. The incorporation of carbon not only enhanced the cyclic stability but also improved the rate capabilities of the prepared FeP/C composite. Chen *et al.* successfully synthesized a hollow double-shell structured bimetallic phosphide (Ni-Fe-P/NC) using a simple phosphidation process with a Prussian blue analog as a precursor.[118] As an anode material for potassium-ion batteries (KIBs), Ni-Fe-P/NC delivered a high capacity of 172.9 mA h g^{-1} after 1600 cycles at a high current density of 500 mA g^{-1}, corresponding to a low capacity decay rate of 0.026% per cycle. The electrode exhibited stable cycling and superior rate performance due to the following reasons: (i) the double-shell structure with a hollow interior cavity, generated from the reaction between PH3 and PBA, provides buffer space to alleviate volume variations during charge and discharge; (ii) the bimetallic phosphide with various active sites anchors polysulfides *via* strong chemisorption; (iii) the nitrogen-doped carbon derived from CN forms defective carbon, exposing more active sites for ion storage. Wang *et al.* successfully designed and synthesized hierarchical FeP nanosheets internally wired with N-doped hollow carbon nanofibers (NeCNF@FeP) through a combination of hydrothermal and phosphidation treatments (Fig. 14a).[119] The NeCNF@FeP composite exhibited a high capacity of 210 mA h g^{-1} at a current density of 0.1 A g^{-1} after 1000 cycles (Fig. 14d). As demonstrated in Fig. 14b and c, the material exhibits excellent electrochemical properties. When employed as an anode material for potassium-ion batteries, the NeCNF@FeP composite demonstrated remarkably reversible capacities, ultra-long cycle life, and superior rate performance for potassium storage. Tao *et al.* successfully synthesized an innovative peapod-like structure with FeP confined in a B/N codoped carbon nanotube array through a facile protocol.[120] The composites exhibit commendable cycling performance, possessing reversible capacities of 111 mA h g^{-1} after 1000 cycles at 1.0 A g^{-1} with negligible capacity loss for FeP@BNCNT electrodes. Zhang *et al.* successfully synthesized porous nitrogen-doped FeP/C nanofibers (P-FeP/C-N NFs), a novel electrode material for potassium-ion batteries (PIBs), using simple electrospinning followed by calcination.[121] In this process, polyacrylonitrile (PAN) and polymethyl methacrylate (PMMA) are used as nitrogen sources and pore-forming agents, respectively. The P-FeP/C-N NFs electrode exhibits excellent electrochemical performance with a discharge capacity of 274.2 mA h g^{-1} (100 mA g^{-1}) after 250 cycles and

171.3 mA h g^{-1} (1000 mA g^{-1}) after 300 cycles, reaching an impressive 150.1 mA h g^{-1} even at 5000 mA g^{-1} discharge capacitance. Zhang *et al.* uniformly anchored hollow FeP nanospheres to a three-dimensional graphene framework to form a flexible and layered porous composite (Fig. 14e).[122] This nanostructure not only established an interconnected conductive network but also provided ample space to accommodate the volume changes of FeP during the potassium storage process, thereby maintaining structural integrity. Benefiting from its unique architecture, the resulting electrode delivered a high reversible capacity of 323 mA h g^{-1} at 100 mA g^{-1}. As illustrated in Fig. 14f and g, the material displays favorable electrochemical properties. After 2000 cycles, an exceptionally high-capacity retention of 97.6% was achieved at 2 A g^{-1} (Fig. 14h).

5 Conclusions

In the field of alkali metal ion batteries, iron phosphide (FeP) has received widespread attention as an anode material due to its high theoretical specific capacity (926 mA h g^{-1}) and suitable operating voltage platform. However, the practical application of FeP is limited by its poor electrical conductivity and significant volume expansion during charging and discharging, which affects its stability and cycle life in real batteries. Therefore, to overcome these challenges, researchers have adopted a variety of strategies, including shortening the electron and ion transport channels by controlling the size of FeP particles to improve the kinetic performance of the batteries; and increasing the electrical conductivity by coating them with highly conductive materials (*e.g.*, carbon); constructing a core–shell or hollow structure to mitigate the effect of volume expansion during charging and discharging; and doping with other elements to increase the material's electrochemical energy storage capacity. In particular, the composite of FeP with carbon materials (FeP/C) is considered to be an effective way to improve the performance of FeP. It has been shown that FeP/C composite nanofibres prepared by electrostatic spinning, carbonization, oxidation, and phosphorization processes exhibit excellent energy storage performance in lithium-ion and sodium-ion batteries.

In addition, the development of composites such as FeP/C@CoP further enhanced the performance of FeP. Through the synergistic effect of internal FeP and external CoP, as well as the fast ion diffusion and accelerated charge transfer provided by the porous carbon matrix, not only the cycling stability of the batteries is improved, but also the reversible capacity of the materials is enhanced. With the continuous research and exploration of the performance of FeP-based materials, more and more innovative structural designs and composite strategies have been proposed. These strategies include compounding FeP with other high-performance materials such as carbon nanotubes, graphene, and transition metal oxides or sulfides to further improve their electrochemical performance and stability. By modulating the microstructures and chemical compositions of the materials, the ion and electron transport channels can be improved at the molecular level, allowing FeP-based materials to exhibit better performance in real batteries.

In summary, the strategic categories for improving the performance of FeP anode materials include carbon coating, heteroatom doping, nanostructuring, core–shell or hollow structures, composite with other materials, and mechanism studies. Among these, carbon coating and heteroatom doping have shown particular promise in enhancing the electrochemical performance of FeP. Future research should focus on further optimizing these strategies, exploring new composite materials, and conducting in-depth mechanism studies to develop more efficient FeP anode materials for alkali metal ion batteries.

Despite the great potential of FeP as an anode material for alkali metal ion batteries, its application in batteries is still not completely clear, especially its reaction mechanism and stability issues in different battery systems. To deeply understand the electrochemical properties of FeP, future studies need to further explore its performance in different types of alkali metal ion batteries, such as lithium-ion, sodium-ion, potassium-ion, *etc.*, with a focus on the mechanism of its performance degradation in long-cycle use. Tools such as density functional theory (DFT) calculations and kinetic analyses can reveal the electrochemical reaction paths, ion diffusion properties, and charge transfer mechanisms of FeP-based materials, thus providing theoretical guidance for optimizing material performance.

With the transformation of global energy structure and the increasingly severe environmental problems, the demand for high-efficiency electrochemical energy storage technology is increasing, which provides a broad prospect for the research of high-performance anode materials such as FeP. To achieve the wide commercial application of FeP-based materials, future research can focus on the following directions: first, exploring more environmentally friendly and low-cost synthesis methods, such as low-temperature synthesis and green solvent method, to reduce the production cost of FeP-based materials; second, further improving the energy density, power density and cycling stability of FeP-based materials by finely tuning their specific surface area, pore structure and electrical conductivity; third, developing novel composite strategies; and third, developing new composite strategies for high-performance negative electrode materials such as FeP. Thirdly, to develop novel composite strategies to combine FeP with new functionalized materials such as polymers and conductive polymers to further improve its electrochemical performance and battery efficiency.

In addition, researchers are also exploring new synthesis methods and material modification strategies for the commercial application of FeP-based materials. For example, non-stoichiometric ratio pure-phase Fe-based hybrid phosphate materials were prepared using solid solution strategies to improve their energy density and cycling stability. It has become a hot research topic to further improve the electrochemical performance of FeP-based materials by introducing transition metal elements (*e.g.*, nickel, cobalt, manganese, *etc.*) or other functionalized components. These studies can not only promote the optimization of the performance of FeP-based materials but also provide new ideas and directions for the future development of alkali metal ion batteries. Especially in

the field of solid-state batteries and high-capacity batteries, FeP-based materials are expected to become one of the core materials for the next-generation high-energy-density batteries by virtue of their unique electrochemical properties. Therefore, further research and development of FeP-based materials, especially in terms of structure optimization, material modification, and performance enhancement, will be of great significance for the advancement of alkali metal ion battery technology and the realisation of commercial applications.

Data availability

The manuscript is a review article. No primary research results, software or code have been included and no new data were generated or analysed as part of this review.

Conflicts of interest

There are no conflicts to declare.

Acknowledgements

This work is supported by the Youth Project of Natural Science Foundation of Hunan Province (2024JJ6413), the Project of the Education Department of Hunan Province (23B0775), Preparation and sodium storage properties of tin-based selenide heterojunction (S202413434025).

Notes and references

1 X. Lin, K. Khosravinia, X. Hu, J. Li and W. Lu, *Prog. Energy Combust. Sci.*, 2021, **87**, 100953.
2 J. P. Pender, G. Jha, D. H. Youn, J. M. Ziegler, I. Andoni, E. J. Choi, A. Heller, B. S. Dunn, P. S. Weiss, R. M. Penner and C. B. Mullins, *ACS Nano*, 2020, **14**, 1243–1295.
3 K. Chayambuka, G. Mulder, D. L. Danilov and P. H. L. Notten, *Adv. Energy Mater.*, 2018, **8**, 1800079.
4 M. Weiss, R. Ruess, J. Kasnatscheew, Y. Levartovsky, N. R. Levy, P. Minnmann, L. Stolz, T. Waldmann, M. Wohlfahrt-Mehrens, D. Aurbach, M. Winter, Y. Ein-Eli and J. Janek, *Adv. Energy Mater.*, 2021, **11**, 2101126.
5 X. Zeng, J. Li and N. Singh, *Crit. Rev. Environ. Sci. Technol.*, 2014, **44**, 1129–1165.
6 Q. Li, D. Yang, H. Chen, X. Lv, Y. Jiang, Y. Feng, X. Rui and Y. Yu, *Susmat*, 2021, **1**, 359–392.
7 Y. Yao, M. Zhu, Z. Zhao, B. Tong, Y. Fan and Z. Hua, *ACS Sustainable Chem. Eng.*, 2018, **6**, 13611–13627.
8 M. Luo, H. Yu, F. Hu, T. Liu, X. Cheng, R. Zheng, Y. Bai, M. Shui and J. Shu, *Chem. Eng. J.*, 2020, **380**, 122557.
9 D. Bin, F. Wang, A. G. Tamirat, L. Suo, Y. Wang, C. Wang and Y. Xia, *Adv. Energy Mater.*, 2018, **8**, 1703008.
10 Z. Bai, Q. Yao, M. Wang, W. Meng, S. Dou, H. K. Liu and N. Wang, *Adv. Energy Mater.*, 2024, **14**(17), 2303788.
11 Y. Fang, L. Xiao, Z. Chen, X. Ai, Y. Cao and H. Yang, *Electrochem. Energy Rev.*, 2018, **1**, 294–323.
12 P. Lyu, X. Liu, J. Qu, J. Zhao, Y. Huo, Z. Qu and Z. Rao, *Energy Storage Mater.*, 2020, **31**, 195–220.
13 T. Yuan, Z. Tan, C. Ma, J. Yang, Z.-F. Ma and S. Zheng, *Adv. Energy Mater.*, 2017, **7**, 1601625.
14 F. Arshad, J. Lin, N. Manurkar, E. Fan, A. Ahmad, M.-N. Tariq, F. Wu, R. Chen and L. Li, *Resour., Conserv. Recycl.*, 2022, **180**, 106164.
15 T. Zhang, C. Li, F. Wang, A. Noori, M. F. Mousavi, X. Xia and Y. Zhang, *Chem. Rec.*, 2022, **22**, e202200083.
16 M. Li, J. Lu, Z. Chen and K. Amine, *Adv. Mater.*, 2018, **30**, 1800561.
17 X. Chang, Y.-M. Zhao, B. Yuan, M. Fan, Q. Meng, Y.-G. Guo and L.-J. Wan, *Sci. China: Chem.*, 2024, **67**, 43–66.
18 L. Zhang, X. Li, M. Yang and W. Chen, *Energy Storage Mater.*, 2021, **41**, 522–545.
19 L. Zhang, X. Li, M. Yang and W. Chen, *Energy Storage Mater.*, 2021, **41**, 522–545.
20 C. Du, Z. Zhao, H. Liu, F. Song, L. Chen, Y. Cheng and Z. Guo, *Chem. Rec.*, 2023, **23**(5), e202300004.
21 M. Lao, Y. Zhang, W. Luo, Q. Yan, W. Sun and S. X. Dou, *Adv. Mater.*, 2017, **29**, 1700622.
22 J. Chen, G. Adit, L. Li, Y. Zhang, D. H. C. Chua and P. S. Lee, *Energy Environ. Mater.*, 2023, **6**(4), e12633.
23 D. Miranda, R. Goncalves, S. Wuttke, C. M. Costa and S. Lanceros-Mendez, *Adv. Energy Mater.*, 2023, **13**(13), 2203874.
24 J. C.-Y. Jung, P.-C. Sui and J. Zhang, *J. Energy Storage*, 2021, **35**, 102217.
25 P. Zhu, D. Gastol, J. Marshall, R. Sommerville, V. Goodship and E. Kendrick, *J. Power Sources*, 2021, **485**, 229321.
26 J. Peng, W. Zhang, Q. Liu, J. Wang, S. Chou, H. Liu and S. Dou, *Adv. Mater.*, 2022, **34**(15), 2108384.
27 Y. Xiao, S. H. Lee and Y.-K. Sun, *Adv. Energy Mater.*, 2017, **7**, 1601329.
28 M. Yuan, H. Liu and F. Ran, *Mater. Today*, 2023, **63**, 360–379.
29 M. Yuan, H. Liu and F. Ran, *Mater. Today*, 2023, **63**, 360–379.
30 G. S. Kamble, T. S. Natarajan, S. S. Patil, M. Thomas, R. K. Chougale, P. D. Sanadi, U. S. Siddharth and Y.-C. Ling, *Nanomaterials*, 2023, **13**, 1528.
31 L. Zhang, C. Zhu, S. Yu, D. Ge and H. Zhou, *J. Energy Chem.*, 2022, **66**, 260–294.
32 L. Zhang, H. Wu and X. Lou, *Adv. Energy Mater.*, 2014, **4**(4), 1300958.
33 W. Zhao, C. Zhao, H. Wu, L. Li and C. Zhang, *J. Energy Storage*, 2024, **81**, 110409.
34 Y. Zhang, B. Wu, G. Mu, C. Ma, D. Mu and F. Wu, *J. Energy Chem.*, 2022, **64**, 615–650.
35 K. R. Sanadi and G. S. Kamble, *Adv. Porous Mater.*, 2018, **6**, 41–44.
36 R. C. Ghaware, N. B. Birajdar, G. S. Kamble and S. S. Kolekar, *Langmuir*, 2024, **40**, 14426–14439.
37 S. R. Bhosale, R. R. Bhosale, G. S. Kamble, S. S. Shukla, S. R. Gadale, R. P. Dhavale and P. V. Anbhule, *Inorg. Chem. Commun.*, 2024, **161**, 112111.
38 W. Cai, C. Yan, Y.-X. Yao, L. Xu, X.-R. Chen, J.-Q. Huang and Q. Zhang, *Angew. Chem., Int. Ed.*, 2021, **60**, 13007–13012.

39 Y. Jiang, M. Hu, D. Zhang, T. Yuan, W. Sun, B. Xu and M. Yan, *Nano Energy*, 2014, **5**, 60–66.
40 J. Liu, Q. Zhang, T. Zhang, J.-T. Li, L. Huang and S.-G. Sun, *Adv. Funct. Mater.*, 2015, **25**, 3599–3605.
41 H. S. Hirsh, Y. Li, D. H. S. Tan, M. Zhang, E. Zhao and Y. S. Meng, *Adv. Energy Mater.*, 2020, **10**, 2001274.
42 G. S. Kamble and Y.-C. Ling, *Sci. Rep.*, 2020, **10**, 12993.
43 T. Perveen, M. Siddiq, N. Shahzad, R. Ihsan, A. Ahmad and M. Shahzad, *Renewable Sustainable Energy Rev.*, 2020, **119**, 109549.
44 M. Peng, K. Shin, L. Jiang, Y. Jin, K. Zeng, X. Zhou and Y. Tang, *Angew. Chem., Int. Ed.*, 2022, **134**(33), e202206770.
45 P. S. Veluri and S. Mitra, *RSC Adv.*, 2016, **6**, 87675–87679.
46 Z. Yan, Z. Sun, A. Li, H. Liu, Z. Guo, L. Zhao, J. Feng and L. Qian, *Chem. Eng. J.*, 2022, **429**, 132249.
47 A. S. Murali, D. Susan Baji, S. Nair and D. Santhanagopalan, *Electrochim. Acta*, 2021, **388**, 138643.
48 J. Liu, T. Zhou, Y. Wang, T. Han, C. Hu and H. Zhang, *Nanoscale*, 2021, **13**, 15624–15630.
49 M. Kundu, D. Xiong, R. Thomas and L. Liu, *J. Alloys Compd.*, 2021, **888**, 161626.
50 S. Boyanov, J. Bernardi, F. Gillot, L. Dupont, M. Womes, J.-M. Tarascon, L. Monconduit and M.-L. Doublet, *Chem. Mater.*, 2006, **18**, 3531–3538.
51 L. Gao, T. Ma, L. Zhang and X. Yang, *J. Solid State Electrochem.*, 2021, **25**, 2055–2063.
52 M. Zhang, H. Wang, Q. Li, J. Feng, Y. Chai, R. Yuan and X. Yang, *Appl. Surf. Sci.*, 2018, **453**, 56–62.
53 X. Xu, J. Feng, J. Liu, F. Lv, R. Hu, F. Fang, L. Yang, L. Ouyang and M. Zhu, *Electrochim. Acta*, 2019, **312**, 224–233.
54 P. Zhou, Q. An, S. Zhu, K. A. Owusu, Q. Li and L. Mai, *Chem. Eng. J.*, 2020, **395**, 125124.
55 F. Han, C. Zhang, J. Yang, G. Ma, K. He and X. Li, *J. Mater. Chem. A*, 2016, **4**, 12781–12789.
56 J. Li, W. Wang, Y. Zhao, M. Chen and Z. Fang, *Energy Technol.*, 2018, **6**, 2312–2318.
57 X. Zhang, W. Ou-Yang, G. Zhu, T. Lu and L. Pan, *Carbon*, 2019, **143**, 116–124.
58 Q. Wang, B. Wang, Z. Zhang, Y. Zhang, J. Peng, Y. Zhang and H. Wu, *Inorg. Chem. Front.*, 2018, **5**, 2605–2614.
59 F. Yang, H. Gao, J. Hao, S. Zhang, P. Li, Y. Liu, J. Chen and Z. Guo, *Adv. Funct. Mater.*, 2019, **29**, 1808291.
60 J. Jiang, C. Wang, J. Liang, J. Zuo and Q. Yang, *Dalton Trans.*, 2015, **44**, 10297–10303.
61 B. Wang, G. Wang, H. Wang and J. Bai, *ChemNanoMat*, 2018, **4**, 924–935.
62 Y. Yang, W. Fu, D. C. Lee, C. Bell, M. Drexler, Z. F. Ma, A. Magasinski, G. Yushin and F. M. Alamgir, *Mater. Today Energy*, 2020, **16**, 100410.
63 B. Hou, Y. Wang, Q. Ning, H. Liang, X. Yang, J. Wang, M. Liu, J. Zhang, X. Wang and X. Wu, *Adv. Electrode Mater.*, 2019, **5**, 1900006.
64 P. Jing, Q. Wang, B. Wang, M. Xiang, H. Jiang, Y. Zhang, Y. Wei, Y. Zhang, H. Wu and H. Liu, *Ceram. Int.*, 2019, **45**, 216–224.
65 X. Xu, J. Liu, Z. Liu, Z. Wang, R. Hu, J. Liu, L. Ouyang and M. Zhu, *Small*, 2018, **14**, 1800793.
66 X. Lin, Y. Ke, X. Peng, C. He, X. Zhao, X. Xiao, X. Lin and J. Nan, *J. Colloid Interface Sci.*, 2023, **634**, 346–356.
67 K. Zhang, Z. Zhu, J. Lin, R. Zhang and C. Zhao, *Appl. Surf. Sci.*, 2020, **500**, 144055.
68 Z. Zheng, H.-H. Wu, H. Liu, Q. Zhang, X. He, S. Yu, V. Petrova, J. Feng, R. Kostecki, P. Liu, D.-L. Peng, M. Liu and M.-S. Wang, *ACS Nano*, 2020, **14**, 9545–9561.
69 X. Li, X. Wang, W. Yang, Z. Zhu, R. Zhao, Q. Li, H. Li, J. Xu, G. Zhao, H. Li and S. Li, *ACS Appl. Mater. Interfaces*, 2019, **11**, 39961–39969.
70 Y. Yang, L. Xu, P. Zhang, W. Wang, J.-J. Zhou, W. Wang, W. Ji, X. Xu, H. Ding and L. Chen, *ACS Appl. Energy Mater.*, 2022, **5**, 6344–6352.
71 C. Wang, J. Yan, T. Li, Z. Lv, X. Hou, Y. Tang, H. Zhang, Q. Zheng and X. Li, *Angew. Chem.*, 2021, **133**, 25217–25223.
72 W. Wang, H. Xu, G. Yu, D. Chen, S. Sun, M. Zhou and J. Chen, *ACS Sustainable Chem. Eng.*, 2021, **5**, 5247–5256.
73 Z. Yan, Z. Sun, K. Yue, A. Li, H. Liu, Z. Guo and L. Qian, *Appl. Surf. Sci.*, 2021, **554**, 149666.
74 M. Zhang, J. Yu, T. Ying, J. Yu, Y. Sun and X. Liu, *J. Alloys Compd.*, 2019, **777**, 860–865.
75 C. Lin, R. Hu, J. Liu, L. Yang, J. Liu, L. Ouyang and M. Zhu, *J. Alloys Compd.*, 2018, **763**, 296–304.
76 G. Li, Y. Ni, H. Guo, X. Li, Z. Wang, G. Yan, J. Wang and W. Peng, *J. Electroanal. Chem.*, 2023, **928**, 117059.
77 J. Yu, Y. He, J. Li, C. Dong, Y. Dai, T. Gao, X. Wang, K. Yue and G. Zhou, *Chem. Eng. J.*, 2023, **477**, 146996.
78 B.-H. Hou, Y.-Y. Wang, Q.-L. Ning, C.-Y. Fan, X.-T. Xi, X. Yang, J. Wang, J.-P. Zhang, X. Wang and X.-L. Wu, *Nanoscale*, 2019, **11**, 1304–1312.
79 T. Li, H. Dong, Z. Shi, W. Liu, X. Li, H. Yue, Y. Yin, B. Li and S. Yang, *J. Solid State Chem.*, 2023, **320**, 123831.
80 M. Gao, X. Liu, H. Yang and Y. Yu, *Sci. China: Chem.*, 2018, **61**, 1151–1158.
81 P. Zhu, Z. Zhang, S. Hao, B. Zhang, P. Zhao, J. Yu, J. Cai, Y. Huang and Z. Yang, *Carbon*, 2018, **139**, 477–485.
82 H. Liu, F. Zou, S. Liao, Y. Pan, Z. Zhao, F. Gu, X. Xu, X. Sang, Y. Han, Z. Bu, L. Qin, Y. Wang, G. Chen, M. Ruan, Q. Li, H. Hu and Q. Li, *J. Phys. Chem. Lett.*, 2024, **15**, 4694–4704.
83 H. Jiang, B. Chen, J. Pan, C. Li, C. Liu, L. Liu, T. Yang, W. Li, H. Li, Y. Wang, L. Chen and M. Chen, *J. Alloys Compd.*, 2017, **728**, 328–336.
84 J. Luo, J. Zhou, H. Zheng, L. Zhu, Q. Fu and K. Tang, *Mater. Lett.*, 2019, **246**, 84–87.
85 Y. Huang, R. Yu, G. Mao, W. Yu, Z. Ding, Y. Cao, J. Zheng, D. Chu and H. Tong, *J. Alloys Compd.*, 2020, **841**, 155670.
86 X. Wang, K. Chen, G. Wang, X. Liu and H. Wang, *ACS Nano*, 2017, **11**, 11602–11616.
87 C. Yao, J. Zha, C. Li, Z. Wang, Y. Shen and A. Xie, *Colloids Surf., A*, 2020, **602**, 125103.
88 J. Zheng, R. Dong, P. Liu, X. Peng, W. Tian, X. Lv, S. Tan and J. Ji, *Surf. Coat. Technol.*, 2021, **421**, 127471.
89 J. Li, Y. Hu, Y. Guo, C. Wang, Z. Huang, S. Luo, S. Yan, M. Qian, Y. Cheng and Y. Ma, *J. Energy Storage*, 2024, **89**, 111642.

90 M. Jiang, L. Ren, Z. Hou, W. Hua, D. Lei, Y. Cao, Y. Zhang and J.-G. Wang, *J. Power Sources*, 2023, **554**, 232334.
91 L. Wang, X. Zhao, S. Dai, Y. Shen and M. Wang, *Electrochim. Acta*, 2019, **314**, 142–150.
92 Y. Von Lim, S. Huang, Y. Zhang, D. Kong, Y. Wang, L. Guo, J. Zhang, Y. Shi, T. P. Chen, L. K. Ang and H. Y. Yang, *Energy Storage Mater.*, 2018, **15**, 98–107.
93 H. Wu, X. Li, L. Chen and Y. Dan, *Batteries Supercaps*, 2019, **2**, 144–152.
94 L. Ren, Y. Huyan, Y. Cao, Z. Luo, Y. Zhang and J.-G. Wang, *Electrochim. Acta*, 2023, **467**, 143077.
95 J. Gao, Y. Li, B. Peng, G. Wang and G. Zhang, *J. Mater. Chem. A*, 2019, **7**, 24199–24204.
96 C. Ma, Z. Fu, C. Deng, X. Liao, Y. He, Z. Ma and H. Xiong, *Chem. Commun.*, 2018, **54**, 11348–11351.
97 S. Shi, C. Sun, X. Yin, L. Shen, Q. Shi, K. Zhao, Y. Zhao and J. Zhang, *Adv. Funct. Mater.*, 2020, **30**, 1909283.
98 F. Han, C. Y. J. Tan and Z. Gao, *ChemElectroChem*, 2016, **3**, 1054–1062.
99 J. Li, Q. Liu, Y. Zhang, J. Jiang, H. B. Wu and X.-Y. Yu, *Chem. Eng. J.*, 2021, **421**, 127776.
100 Z. Li, H. Zhao, Z. Du, L. Zhao, J. Wang and Z. Zhang, *J. Power Sources*, 2020, **465**, 228253.
101 H. M. Saleem, M. Jamil, M. Tabish, A. H. Khoja, A. Li, D. Wang and H. Song, *ACS Appl. Energy Mater.*, 2023, **6**, 9885–9896.
102 S. Shi, Z. Li, L. Shen, X. Yin, Y. Liu, G. Chang, J. Wang, S. Xu, J. Zhang and Y. Zhao, *Energy Storage Mater.*, 2020, **29**, 78–83.
103 L. Zhao, J. Li, B. Peng, G. Wang, L. Yu, Y. Guo, L. Shi and G. Zhang, *ChemElectroChem*, 2022, **9**, e202200519.
104 S. Park, C. W. Kim, K. S. Lee, S. J. Hwang and Y. Piao, *Nanoscale*, 2023, **15**, 14155–14164.
105 J. Jiang, C. Ma, W. Zhang, Y. He, X. Li and X. Yuan, *Chem. Eng. J.*, 2022, **429**, 132271.
106 Y. Jiang, W. Zhang, Y. Yang, Y. He, J. Wang, X. Yang, X. Liao and Z. Ma, *ChemNanoMat*, 2018, **4**, 309–315.
107 Y. Wang, Y. V. Lim, S. Huang, M. Ding, D. Kong, Y. Pei, T. Xu, Y. Shi, X. Li and H. Y. Yang, *Nanoscale*, 2020, **12**, 4341–4351.
108 Q. Li, J. Yuan, Q. Tan, G. Wang, S. Feng, Q. Liu and Q. Wang, *New J. Chem.*, 2020, **44**, 5396–5403.
109 Y. Wang, Q. Fu, C. Li, H. Li and H. Tang, *ACS Sustainable Chem. Eng.*, 2018, **6**(11), 15083–15091.
110 S. Park, D. Kim, M. Jang, T. Hwang, S. J. Hwang and Y. Piao, *Nanoscale*, 2022, **14**, 6184–6194.
111 Z. Li, L. Zhang, X. Ge, C. Li, S. Dong, C. Wang and L. Yin, *Nano Energy*, 2017, **32**, 494–502.
112 L. Han, M. Zhang, H. Wang, P. Li, W. Wei, J. Shi, M. Huang, Z. Shi, W. Liu and S. Chen, *Nanoscale*, 2020, **12**, 24477–24487.
113 Z. Xiao, L. Gao and S. Li, *Materials*, 2024, **17**, 1616.
114 T. Mao, Z. Hong, H. Ding, J. Li, Y. Xia, Z. Zhou and G. Yue, *Coatings*, 2023, **13**, 2056.
115 C. Ma, Y. Hou, K. Jiang, L. Zhao, T. Olsen, Y. Fan, J. Jiang, Z. Xu, Z. Ma, D. Legut, H. Xiong and X.-Z. Yuan, *Chem. Eng. J.*, 2021, **413**, 127449.
116 Q. Tan, W. Zhao, K. Han, P. Li, W. (Alex) Wang, D. He, Z. Liu, Q. Yu, M. Qin and X. Qu, *J. Mater. Chem. A*, 2019, **7**, 15673–15682.
117 W. Li, B. Yan, H. Fan, C. Zhang, H. Xu, X. Cheng, Z. Li, G. Jia, S. An and X. Qiu, *ACS Appl. Mater. Interfaces*, 2019, **11**, 22364–22370.
118 X. Chen, S. Zeng, H. Muheiyati, Y. Zhai, C. Li, X. Ding, L. Wang, D. Wang, L. Xu, Y. He and Y. Qian, *ACS Energy Lett.*, 2019, **4**, 1496–1504.
119 X. Wang, J. Ma, J. Wang and X. Li, *J. Alloys Compd.*, 2020, **821**, 153268.
120 X. Tao, Z. Zhang, Z. Li, S. Xiong, S. Wang, F. Gao, C. Wang and L. Hou, *ACS Appl. Mater. Interfaces*, 2024, **16**, 772–783.
121 W. Zhang, Y. Liu, Z. Ye, M. Yang, Q. Luo, J. Dai, Q. Wang and L. Liu, *J. Cent. South Univ.*, 2023, **30**, 3248–3259.
122 Z. Zhang, C. Wu, Z. Chen, H. Li, H. Cao, X. Luo, Z. Fang and Y. Zhu, *J. Mater. Chem. A*, 2020, **8**, 3369–3378.